Large-Scale Structure of Trace Gas and Aerosol Distributions over the Western Pacific Ocean during TRACE-P

Meigen Zhang[1,2], Itsushi Uno[1,3], Gregory R. Carmichael[4], Hajime Akimoto[1], Zifa Wang[1,2], Youhua Tang[4], Jung-Hun Woo[4], David G. Streets[5], Glen W. Sachse[6], Melody A. Avery[6], Rodney J. Weber[7], and Robert W. Talbot[8]

Abstract. The Models-3 Community Multi-scale Air Quality modeling system (CMAQ) coupled with the Regional Atmospheric Modeling System (RAMS) is used to analyze the Asian continental outflow of carbon monoxide (CO), ozone (O_3), and aerosol sulfate (SO_4^{2-}) to the western Pacific Ocean during the period March 17-24 of 2001. In this time period 8 airborne observations (DC-8 flights 11-14 and P-3B flights 13-16) of the NASA Transport and Chemical Evolution over the Pacific (TRACE-P) mission were being conducted over a broad area covering Hong Kong, Okinawa, East China Sea and southern Japan. Comparison of model results with observations shows that the model reproduces the main observed features of CO, O_3 and SO_4^{2-}, including horizontal and vertical gradients, of the Asian pollution outflow over the western Pacific. Model results show that the fast boundary outflow from Asia to the western Pacific is largely restricted to the middle latitudes, and the maximum outflow fluxes are in the lower free atmosphere (3-6 km) north of 25°N. Simulations with and without biomass burning emissions are conducted to quantify the impacts of biomass burning on tropospheric concentrations of CO and O_3. Biomass burning is found to contribute more than 50% of the CO concentrations and up to 40% of the O_3 concentrations in the boundary layer over the major source regions. The largest percentage contributions to CO and O_3 levels (up to 40% and 30% respectively) over the western Pacific are in the lower free troposphere (2-6 km).

1. Introduction

The rapid industrilization now taking place in Asia is expected to have important implications for global atmospheric chemistry over the next decades [*Berntsen et al*., 1996]. Transport and chemical evolution of trace gases and aerosols from the Asian continent significantly alter the composition of the remote Pacific troposphere [e.g., *Uematsu et al.,* 1983; *Jaffe et al.,* 1997; *Crawford et al*., 1997; *Talbot et al.,* 1997; *Wang et al.,* 2000; *Uno et al*., 2001], and there is growing observational envidence for an Asian impact extending to North America [e.g., *Jaffe et al.,* 1999; *Berntsen et al.,* 1999; *Yienger et al*., 2000]. *Kato and Akimoto* [1992] estimated that the emissions of nitrogen oxides (NO_x) in East Asia have increased by 58% from 1975 (2.05 TgN/yr) to 1987 (3.25TgN/yr), and *van Aardenne et al.* [1999] predicted an increase of almost four-fold in NO_x emissions from 1999 to

[1] Frontier Research System for Global Change, Yokohama 236-0061, Japan
[2] State Key Laboratory of Atmospheric Boundary Layer Physics and Atmospheric Chemistry, Institute of Atmospheric Physics, Chinese Academy of Sciences, Beijing, China
[3] Research Institute for Applied Mechanics, Kyushu University, Kasuga Park 6-1, Kasuga 816-8580, Japan
[4] Center for Global and Regional Environmental Research and Department of Chemical and Biochemical Engineering, Univesity of Iowa, Iowa City, Iowa
[5] Decision and Information Sciences Division, Argonne National Laboratory, Illinois
[6] NASA Langley Research Center, Hampton, Virginia
[7] Georgia Institute of Technology, Atlanta
[8] Institute for the Study of Earth, Oceans, and Space, University of New Hampshire, Durham

2020. Gas-phase emissions of organics, NO_x and sulfur dioxide (SO_2) from the Asian continent undergo photooxidation as air masses are advected eastward over the Pacific. SO_2 is perhaps the most important individual precursor compound for secondary matter in the atmosphere, and the conversion of SO_2 to aerosol sulfate (SO_4^{2-}) occurs via multiple pathways, including gas phase oxidation to sulfuric acid (H_2SO_4) followed by condensation into the particulate phase, aqueous phase oxidation in cloud or fog droplets, and various reactions on the surfaces or inside aerosol particles. In the continental outflow region, primary aerosols of mineral dust and sea salt origin, and the continental anthropogenic aerosols, are transformed by gas-aerosol interactions [*Dentener et al*., 1996; *Song and Carmichael*, 2001]. There is a clear need to better understand the chemical processing of emissions over Asia and the mechanisms for export of the pollution to the global atmosphere.

In this study we analyze the Asian outflow of carbon monoxide (CO), ozone (O_3) and SO_4^{2-} in the springtime by using the Models-3 Community Multi-scale Air Quality modeling system (CMAQ) with meteorological fields from the Regional Atmospheric Modeling System (RAMS). This modeling system was used to analyze data obtained during the Transport and Chemical Evolution over the Pacific (TRACE-P) aircraft mission. This experiment was conducted by the Global Tropospheric Experiment (GTE) of the National Aeronautics and Space Administration (NASA) in March-April 2001. The period March 17 to 24, 2001, when two aircrafts (DC-8 and P-3B) made intensive observations over the western Pacific covering Hong Kong, Okinawa, East China Sea and southern Japan, is analyzed in this paper, with the focus on the investigation of the multi-scale pollutant transport associated with two western Pacific wave cyclones. This week was chosen because the associated frontal lifting, followed by westerly transport in the lower troposphere, are the principal processes responsible for export of both anthropogenic and biomass burning pollution in East Asia. The analysis of the observations during this period using the three-dimensional regional scale transport/chemistry model provides an excellent case study to both test the model and to provide a regional context of how pollutants are transported out of East Asia. A comprehensive evaluation of our regional-scale analysis of the entire TRACE-P intensive observations is the focus of a separate paper [*Carmichael et al.,* this issue].

Biomass burning emissions in the tropics has been reported to exert a strong influence on the abundance of trace gases in the atmosphere [e.g., *Crutzen and Andreae, 1990; Galanter et al., 2000*], and tropical Asia is a region of extensive biomass burning [e.g., *Christopher et al.,* 1998]. East-central India and the region containing Thailand, Laos, Cambodia and Vietnam are identified as the two major areas of biomass burning in India and Southeast Asia. Biomass burning was active during March 17 to 24, and air masses heavily influenced by biomass burning emissions were sampled during this period [*Tang et al.,* this issue]. For investigating the impacts of biomass burning on tropospheric concentrations of CO and O_3 over the western Pacific and its contribution to the Asian outflow, simulations with and without biomass burning emissions were carried out.

This paper is divided into four sections. We briefly describe the model, its initial and boundary conditions, and emission inventories in section 2. In section 3 we firstly compare model results with observations from the TRACE-P mission, then discuss temporal and spatial concentration distributions of CO, O_3 and SO_4^{2-} and their export pathways, and finally analyze biomass burning impacts on CO and O_3 concentrations and budgets. Conclusions are presented in section 4.

2. Model Description

CMAQ is a Eulerian-type model developed in the U.S. Environmental Protection Agency to address tropospheric ozone, acid deposition, visibility, particulate matter and other pollutant issues in the context of a "one atmosphere" perspective where complex interactions between atmospheric pollutants and regional and urban scales are confronted. It is designed to be flexible so that different levels of model configuration can be achieved. The current version of CMAQ uses meteorological fields from the Regional Atmospheric Modeling System [RAMS; *Pielke et al*., 1992] version 4.3 instead of its default meteorological driver - the Mesoscale Modeling System (MM5), and is configured with the chemical mechanism of the Regional Acid Deposition version 2 [RADM2; *Stockwell et al.*, 1990], extended to include the four-product Carter isoprene mechanism [*Carter*, 1996], and aerosol processes from direct emissions and production from sulfur dioxide, long-chain alkanes, alkyl-substituted benzene, etc. To depict aerosol evolution processes in the atmosphere, the Regional Particulate Model [RPM; *Binkowski and Shankar*, 1995] module was included. In this module the particle size distribution is represented as the superposition of three lognormal sub-distributions, and the processes of coagulation, particle growth by the addition of new mass, particle formation, dry deposition, scavenging, and aerosol chemistry are included. Other important components to the CMAQ configuration are: (1) advection algorithm with Piece-wise Parabolic Method [*Colella and Woodward*, 1984]; (2) horizontal diffusion with scale dependent diffusivity; (3) vertical diffusion with a local scheme based on the semi-implicit K-theory; (4) Mass conservation adjustment [*Byun, 1999*]; (5) emissions injected in the vertical diffusion module; (6) deposition flux as bottom conditions for the vertical diffusion; and (7) QSSA gas-phase reaction solver. A general description of CMAQ and its capabilities are given in *Byun and Ching* [1999]. CMAQ coupled with RAMS has recently been successfully applied to East Asia to simulate tropospheric ozone [*Zhang et al.,* 2002].

For CMAQ, the anthropogenic emissions of nitrogen oxides, carbon monoxide, volatile organic compounds (VOCs) and SO_2 were obtained from the emission inventory of 1^ox1^o specially prepared by scientists at the Center for Global and Regional Environmental Research at the University of Iowa [*Streets et al.,* this issue] to support TRACE-P and ACE-Asia (the Aerosol Characterization Experiment – Asia) and from the

Emission Database for Global Atmospheric Research [EDGAR; *Oliver et al.,* 1996]. NO_x emissions from soils and natural hydrocarbon emissions were obtained from the Global Emissions Inventory Activity (GEIA) 1°x1° monthly global inventory [*Benkovitz,* 1996] for the month of March. VOC emissions were apportioned appropriately among the lumped-hydrocarbon categories used in RADM2. SO_2 emissions arising from volcanoes are based on the estimates by *Streets et al*. [this issue]. In this study it is assumed that 5% SO_2 emitted was in the form of H_2SO_4.

Biomass burning is an important source of CO and NO_x in Asia in the springtime, because spring is the dry season, and there is extensive biomass burning in Southeast Asia and India, mainly due to burning of agricultural waste (rice straw) and deforestation [*Nguyen et al.,* 1994]. Biomass burning emissions include sources from forest wildfires, deforestation, savanna burning, slash-and-burn agriculture, and agricultural waste burning. In this study emissions of CO from biomass burning were based on the inventory of a 1^ox1^o spatial resolution and daily temporal resolution estimated using fire count derived from the AVHRR satellite images [*Woo et al.,* this issue]. Biomass burning emissions for other tracers are estimated by applying mean observed tracer emission ratios relative to CO [*Wang et al.,* 1998], e.g., average molar emission ratio of 4.5% for NO_x to CO, 0.55% for ethane to CO, and 0.15% for propane to CO.

The total emissions used in this study and their sources from biomass burning emissions are summarized in Table 1. The table shows that China has the largest emissions of NO_x, CO, SO_2 and some hydrocarbon species, and CO emissions from biomass burning contribute ~50% to the total CO emissions. In Southeast Asia and part of India biomass burning emitted CO takes more than 80% of CO emissions there.

RAMS is a highly versatile numerical code developed at Colorado State University for simulating and forecasting meteorological phenomena. In this study it is used to simulate the regional scale three-dimensional meteorological field including boundary-layer turbulence, cloud and precipitation. RAMS includes the Kuo-type cumulus parameterization to represent the subgrid scale convective cumulus and the Kessler-type microphysics model [*Walko et al*., 1995]. Microphysics module in RAMS is capable of simulating meso-scale clouds and precipitation phenomena. The surface flux calculation module in RAMS [*Louis,* 1979] was improved based on the result of *Uno et al.* [1995]. Level 2.5 turbulent closure model [*Mellor and Yamada,* 1974] and LEAF [Land Ecosystem Atmosphere Feedback model; *Lee,* 1992] soil-vegetation model are also used for the simulation. A general description of RAMS and its capabilities are given in *Pielke et al*. (1992).

In this study RAMS was exercised in a four-dimensional data assimilation mode using analysis nudging with re-initialization every four days, leaving the first 24 hours as the initialization period. The three-dimensional meteorological

fields for RAMS were obtained from the European Center for Medium-Range Weather Forecasts (ECMWF) analyzed datasets, and were available every six hours with 1°×1° resolution. Sea Surface Temperatures (SST) for RAMS were based on weekly mean values and observed monthly snow-cover information as the boundary conditions for the RAMS calculation.

The model domain (shown in Figure 1) is 8000x5600 km^2 (outside region) for RAMS and 6240x5440 km^2 (inside region) for CMAQ on a rotated polar-stereographic map projection centered at (25°N, 115°E) with 80 km mesh. RAMS and CMAQ have the same model height. For RAMS there are 23 vertical layers in the σ_z coordinates system unequally spaced from the ground to ~23 km, with about 9 layers concentrated in the lowest 2 km of the atmosphere in order to resolve the planetary boundary layer, while there are 14 levels for CMAQ with the lowest 7 layers being the same as those in RAMS.

Initial and boundary conditions of species in CMAQ were chosen to reflect the East Asian situation. Recent measurements were used whenever possible. To evaluate the impact of the anthropogenic emissions on the distributions of trace gases and aerosols, the initial and boundary conditions were generally chosen at the lower end of their observed range (e.g., the northern and western boundary conditions for O_3, CO, NO_2, SO_2 and SO_4^{2-} were 30 ppbv, 120 ppbv, 0.2 ppbv, 0.3 ppbv and 1 ug/m^3, respectively) so as to allow the emissions and chemical reactions to bring them closer to their actual values during the initialization period [*Liu et al.,* 1996; *Carmichael et al.,* 1998].

The upper boundary of CMAQ is located in the lower stratosphere. Stratospheric influence on tropospheric ozone is parameterized by specifying the initial and boundary conditions at the top 3 altitude levels of the model to values proportional to potential vorticity (PV). The proportional coefficient is assumed to be constant. For ozone, 50 ppbv per PV unit is adopted according to the studies by *Ebel et al*. [1991] and *Beekmann et al*. [1994], where the PV unit is 10^{-6} $Km^2kg^{-1}s^{-1}$.

3. Results and Discussion

The simulation period covered February 22 to May 5, 2001 with a starting time at 0000 Z on February 22, i.e., 0900 JST (Japanese Standard Time). In this paper model results for the period of March 17 to 24, 2001 are presented and discussed in order to quantify the chemical and dynamical evolution of the Asian continental outflow over the western Pacific associated with two traveling wave cyclones. For investigating the impacts of biomass burning on tropospheric concentrations of CO and O_3, one additional simulation was carried out by switching off the emissions from biomass burning. This method of estimating the influences of biomass burning emissions on pollutant distributions has been used by a number of groups [e.g., *Galanter et al.*, 2000 and references there in].

We recognize that the attribution of the role of biomass burning emissions determined in this manner (especially for O_3) may not be precise due to non-linearities in the photochemical oxidant cycle. However, our analysis has shown that model-derived results are very consistent with the observed enhancements as discussed in *Tang et al.,* [this issue].

3.1. Comparison with Observations from the TRACE-P mission in the study period

In comparing the model results with the TRACE-P aircraft observations, we sampled the model along the flight tracks and with a 1-hour temporal resolution. The observed data are 5-minute averaged. *Carmichael et al.* [this issue] compared the meteorological parameters (such as wind speed and direction, temperature and water mixing ratio) simulated by RAMS with airborne measurements and showed that the modeled meteorology reproduced quantitatively most of the major observed features. For example the correlation coefficients for wind speed, temperature and relative humidity each exceeded 0.9 for all TRACE-P observation points for altitudes below ~5 km. A TRACE-P mission-wide perspective that compares the observed values of 33 different chemical species and photolysis rates with regional model values is presented in *Carmichael et al.* [this issue]. We present here a more focused evaluation of CMAQ simulated mixing ratios of CO, O_3 and SO_4^{2-} with observations from the TRACE-P mission during the period of March 17 to 24, 2001. We focus on these three species as they represent major components in the Asian outflow, and reflect a variety of sources and processes. For example, CO arises from a wide variety of combustion sources, including a large contribution from biomass burning, ozone reflects both VOC and NO_x emissions as well as the photochemical processes, and sulfate reflects largely fuel combustion and volcanic emissions of precursor SO_2 as well as in-cloud chemical and removal processes. Additional evaluation of model results with time series of O_3 concentrations measured at two Japanese remote sites Ochiishi and Hateruma during TRACE-P is also presented.

Figure 2 shows the horizontal DC-8 and P-3B flight tracks in the study period, and Figures 3, 4 and 5 present the time series of observed and simulated concentrations of CO, O_3 and SO_4^{2-} along these flights.

On March 17 the DC-8 (flight 11) and P-3B (flight 13) flew from Hong Kong to Okinawa. Figures 2a and 3a show that the DC-8 observed elevated CO mixing ratios near Hong-Kong (indicated by A-1) at an altitude of ~2 km, and in a region south of Shikoku Island of Japan (indicated by A-2) at a height of 3~4 km. In figures 2a and 3b we find that the P-3B observed high CO concentrations (exceeding 400 ppbv) over the Yellow Sea (indicated by A-3). From Figures 3a and 3b we find that the model reproduces the temporal and spatial variations of CO concentrations reasonably well; e.g., the timing and locations of the CO spikes are very well captured, but the model tends to underestimate the peak values. Analysis of the model results shows that biomass burning contributes a maximum of 103 ppbv to the elevated CO concentrations at A-2 (Figure 3a). The high concentrations of CO at A-3 (Figure 3b) reflect a combination of contributions from Shanghai and

from biomass burning. For reference in Figure 3 we include the CO mixing ratios predicted by the Sulfur Transport Eulerian Model (STEM) using the same meteorological fields and emissions as discussed in *Carmichael et al. (this issue)*. As shown the CO levels predicted by CMAQ are nearly identical to those predicted by STEM.

The time series of O_3 mixing ratios in Figures 4a and 4b show that north of 25°N (after ~1300 JST) O_3 concentrations increase with height (above 6 km) in the case of the DC-8 observations, while they do not change much in the P-3B observations as its ceiling height is ~6 km. The model captures these features. South of 25°N (before ~1300 JST in Figure 4a) the DC-8 observed low O_3 concentrations of ~20 ppbv above 9 km, but the model predicts much higher values (>80 ppbv), due to a strong stratospheric contribution at this time in the model. In general the calculated O_3 concentrations agree better with observations on the P-3B than on the DC-8, with a general tendency to overpredict at high altitudes, especially at low latitudes (e.g. Figure 4a before ~1300 JST). For quantifying the effect of upper air transport, we made further analysis by comparing the DC-8 observed O_3 and CMAQ simulated O_3 concentrations within the region of altitude < 8 km (the figure not shown here), we did not see a strong overprediction of O_3 in the troposphere below. While overprediction of O_3 approximately up to 100-140 ppbv is seen in the regions of latitude > 30°N and altitude > 8 km, and for latitude < 30°N and altitude > 4 km. This overestimation reflects a too strong stratospheric input in the model and related downward transport, and implies the limitation of the assumed PV-O_3 relationship (although the model did capture the O_3 maximum recorded by the DC-8 on March 21 (Figure 4e)). Another possibility to cause the O_3 overestimation is that we did not account for the heterogeneous reaction of ozone on dust, which could provide an important ozone sink in Asian continental plumes (10 to 40%) as proposed by *Zhang and Carmichael* [1999] and *Dentener et al.* [1996].

In contrast to the observations of CO and O_3, SO_4^{2-} mixing ratios are high in the boundary layer and typically decrease sharply with height above the boundary layer (Figures 5a and 5b). The model accurately represents this vertical behavior, but tends to overpredict sulfate levels in the boundary layer during this period. This over-prediction in the boundary layer is not observed when we look at the entire TRACE-P period, but may reflect the difficulties in modeling the complex vertical structures in the lowest 2 km of the cloudy marine atmosphere that were observed during this 17 to 24 March period as discussed by *Tu et al.* [this issue].

On the next day the DC-8 (flight 12) observed elevated CO and SO_4^{2-} mixing ratios in the boundary layer in the Taiwan Strait (B-1 in Figures 2b, 3c and 5c). The model reproduces these high concentrations (Figures 3c and 5c), and shows that both anthropogenic and biomass burning emissions contribute to the CO spikes. At B-2 the P-3B (flight 14) observed very high concentrations of CO and SO_4^{2-}, and the model attributes these elevated values to emissions from Shanghai. Both flights observed elevated CO, O_3 and SO_4^{2-} concentrations in the B-3 region, which was located at the backside of cold front (post-frontal boundary layer outflow). Figures 3d, 4d and 5d show that the model reproduces the observed mixing ratios of CO,

O_3 and SO_4^{2-} very well except at B-2 where CO concentrations are greatly underestimated. This underestimation may be due in part to the incapability of the model with 80 km horizontal grid to resolve this urban plume.

On March 21 the DC-8 (flight 13) observed elevated concentrations of CO, O_3 and SO_4^{2-} near the China coast (at C-1 in Figure 2c CO was as high as 1000 ppbv, O_3 reached 120 ppbv and SO_4^{2-} exceeded 40 ug/m^3) and over the ocean south of Japan (at C-2 in Figure 2c with CO levels up to 400 ppbv and SO_4^{2-} up to 20 ug/m^3). Analyses of the modeled horizontal distributions of these species during the period show that these high concentrations are associated with pollution outflow from the Shanghai area (Figures 3e, 4e and 5e). Over the Japan Islands the DC-8 observed high O_3 levels ranging from 150 to 400 ppbv at the altitude of 3-11 km, which is due to subsidence of stratospheric air on the north side of the jet stream, and the model captured this feature (cf. Figure 4e).

During flight 15 the P-3B made observations mainly in the frontal zone. Observed CO values were rather low both behind and beyond the front (mostly in the 100-200 ppbv range). The vertical ascent at 40^{o}N fell within the frontal zone and showed no gradient in CO (120 ppbv) and O_3 (60 ppbv) (Figures 3f and 4f). During this flight the P-3B encountered strong pollution within the boundary layer (at C-3 in Figures 2c, 3f and 4f), and model analysis indicates that the high CO concentrations were associated with Asian outflow. The elevated SO_4^{2-} mixing ratios were found to be associated with emissions from the Miyakejima volcano, located to the south of Tokyo. Figures 3f, 4f and 5f show good agreement between observations and simulations, and according to the model biomass burning played little role in this observation area at this time.

On March 24 the DC-8 (flight 14) mainly flew to the south of Japan, while the P-3B (flight 16) flew to the Japan Sea and the south coast of Japan. This day also included an inter-comparison flight with the DC8 (see Figure 2d). Along the southern coast of Japan both aircrafts observed high CO concentrations in the boundary layer (indicated by D-1 in Figure 2d) due to surface outflow. Model results show the outflow was a combination of industrial and biomass burning influences (Figures 3g and 3h). In the same area SO_4^{2-} mixing ratios were high due to the heavy influence of Miyakejima volcano, and the model reproduces these high values reasonably well (Figures 5g and 5h).

During this day the DC-8 encountered strong pollution (CO - 200 ppbv, O_3 - 80 ppbv) in the upper troposphere at D-2 and D-3 shown in Figure 2d. The observed high mixing ratios of C_2Cl_4 and CH_3CN in this layer reflects a combination of industrial and biomass burning influences. However, the model could not reproduce the high CO concentrations (Figure 3g) due to either an underestimation of biomass burning emissions or to long-range transport from outside the model domain.

Figure 6 shows the time variations of hourly averaged ozone mixing ratios measured at two remote Japanese sites Ochiishi (Figure 6a) and Hateruma (Figure 6b). Also shown are the results from the model for the lowest model layer (approximately 150 m above the ground). The locations of the observation sites are shown in Figure 1. In most cases the

model is able to reproduce the synoptic features in the observed ozone. The timing of peaks and low ozone levels were reasonably well captured at both sites. We can see in Figure 6b that the model sometimes overpredicts the O3 concentrations, but not systematically. We think that the overprediction is associated with the exchange of different air masses (i.e., maritime and continental air masses) which CMAQ can not retrieve well because of large gird size of 80 km.

3.2. Transport and Chemical Evolution of Asian Outflow in the Boundary Layer

Figures 7, 8 and 9 present the horizontal distributions of hourly-averaged CO, O_3 and SO_4^{2-} mixing ratios in the boundary layer at 1200 JST (0300 Z) on March 17, 18, 20, 21, 23 and 24, 2001. Also shown are the percentage contributions of biomass burning to CO and O_3 (Figures 7 and 8), and wind vectors at an altitude of ~500 m (Figure 9). In figures 7 and 8 the percentage contribution to CO or O_3 concentrations from biomass burning was calculated as,

$$(C_{base} - C_{test}) / C_{base} * 100\%,$$

where C_{base} and C_{test} is the mixing ratios of CO or O_3 from the simulations with and without biomass burning emissions, respectively.

During the period of interest the dominant meteorological features were associated with two traveling low-pressure systems. On March 17 a developing wave cyclone was located east of Shanghai, and an anticyclone was centered just east of Tokyo. The wave cyclone intensified during the day and moved eastward, and its associated cold front also swept toward the east. On March 18 the wave cyclone was located just off the northeast coast of Japan; the central pressure reached 996 hPa and was moving towards the northeast. A similar wave cyclone developed and intensified between March 20 and March 23, but traveled eastward. At this time a subtropical high was located over northern Philippines, producing northeasterly winds over Southeast Asia. In addition, there was a large low-pressure area between northeast China and the Sea of Okhotsk, which was quite stationary.

Figure 7a shows that the area with CO values larger than 330 ppbv covered Southeast Asia and southern, eastern and central China on March 17. These elevated levels generally correspond to areas of intense biomass burning and enhanced industrial and transportation activity. We estimate that biomass burning contributed more than 60% to the CO levels over Southeast Asia and southern China. Biomass contributions exceeding 20% extends over a broad region from central and eastern China to Okinawa and Kyushu areas in Japan.

CO was transported towards the east and northeast as the wave cyclone moved towards the east. On March 18 the area with CO greater than 330 ppbv extended to Okinawa. Figure 7b clearly shows a high CO (>250 ppbv) belt extending from Shanghai area to the southern coast of Japan (140^oE). From Figure 7c we can see that the highest CO concentrations are over the high emissions regions in Southeast Asia and central and eastern China. The influence of Asian outflow is clearly

seen over Kyushu Islands of Japan and over the western Pacific.

On March 21 a low-pressure system was centered over northern Japan. A cold front extended from it; first towards the southeast along 150°E, and then southwest towards Taiwan. A developing low-pressure area was located over northeastern Asia. CO was transported from the Shanghai area to the western Pacific in the westerly flow, and CO mixing ratios greater than 330 ppbv covered the East China Sea and Okinawa (Figure 7d). Both the DC-8 and P-3B observed high CO values in these areas (Figure 2d).

Ozone distributions are presented in Figure 8 and the general patterns are similar to those for CO. In addition along the major export pathway (i.e., the pollution belt) O_3 is correlated with CO. O_3 produced due to biomass burning emissions contribute more than 40% to O_3 levels downwind of the source regions. Off the southern coast of Japan, high O_3 mixing ratios (>75 ppbv with 10% contributions from biomass burning) are also well correlated with elevated CO concentrations (up to 250 ppbv), and 20% is from biomass burning.

Ambient SO_4^{2-} comes mostly from the oxidation of SO_2 released into the lower atmosphere as a result of fossil fuel combustion or volcanic eruptions. The oxidation process of SO_2 to SO_4^{2-} involves complex chemical mechanisms both in the gas and aqueous (cloud) phases. As shown in Figure 9a elevated SO_4^{2-} concentrations are mainly seen in Sichuan, Shanghai and Taiwan areas in association with high anthropogenic emissions, while high levels over Tokyo and the ocean areas to the east, are attributed to the emission from the Miyakejima volcano. In Southeast Asia SO_4^{2-} concentrations are generally low. From Figures 9e-9f we find that the emissions from the Miyakejima volcano play an important role in maintaining high SO_4^{2-} concentrations over the western Pacific, and strong eastward/northeastward transport of SO_4^{2-} and its precursors from the Asian continent contributes to high SO_4^{2-} levels over the East China Sea and even over northern Japan (Figure 9c).

3.3. Vertical Structure of CO, O_3 and SO_4^{2-} along the DC-8 Flight Tracks in the study period

Figure 10 shows the model simulated altitude-time cross-sections of CO concentrations and its percent contributions of biomass burning along the DC-8 flight tracks. We find that the highest CO concentrations are in the middle latitudes, below 2 km (cf. Figure 2 for the DC-8 flight coverage), and they mainly arise from anthropogenic sources. The largest percent contributions of biomass burning to CO concentrations are in the layer of 2-6 km. High CO values are also found in free atmosphere, where contributions from biomass burning range from 20-50%.

The vertical distribution of ozone and its percent contributions from biomass burning along the DC8 flight tracks are shown in Figure 11**.** Elevated O_3 concentrations are typically found in the boundary layer, where CO concentrations are also generally high. The good correlation of O_3 and CO implies that photochemical production of O_3 within the boundary layer is significant. The figure also shows high

O_3 values in the upper layers above 30°N, due to a decrease in the height of the tropopause with latitude, and subsidence of stratospheric air are on the north side of the jet stream. In low latitudes the tropopause is high and O_3 levels are low in the upper troposphere. The largest biomass burning contributions to O_3 levels are found in the free troposphere, which is consistent with biomass burning contributions to CO levels shown in Figure 10.

Figure 12 shows the vertical distributions of SO_4^{2-} along the DC8 flight tracks. High SO_4^{2-} concentrations are mainly found below 2 km. A strong influence of the Miyakejima volcano on SO_4^{2-} concentrations was observed and simulated over the southern coast of Japan on March 24 (Figures 2f and 12d).

Figures 10, 11 and 12 show that CO, O_3 and SO_4^{2-} concentrations exhibit large temporal and spatial variations in the vertical because of their different sources and sinks, while they are well correlated in the boundary layer as the anthropogenic emissions are their dominant sources. Biomass burning has important impacts on CO and O_3 concentrations in the free atmosphere. The mechanism for biomass burning contributing to CO and O_3 concentrations in the free troposphere will be discussed in the next section.

3.4. Pathways for the Export of CO, O_3 and SO_4^{2-} from Asia

Figure 13 shows the mean horizontal fluxes of CO, O_3 and SO_4^{2-} integrated over the tropospheric column (0 ~ 9 km for CO and SO_4^{2-} while 0 ~ 2.5 km for O_3) for the period of study. Figure 14 presents the average vertical distributions of CO, O_3 and SO_4^{2-} concentrations and their zonal fluxes along ~125°E. Also shown in Figures 14b and 14d are biomass burning contributions to CO and O_3 fluxes, respectively. In Figure 13 we find that the main export pathway for Asian pollution to the western Pacific is in the westerly flow north of 25°N. Wind fields in Figure 9 clearly show a convergence zone in the boundary layer over central and eastern China, where air masses from the north, driven by monsoon winds, encounter oceanic air masses from the south. This convergence zone plays an important role in the springtime export of pollution from the Asian continent. Strong westerlies are the prevailing meteorological pattern at altitudes above 2 km and at latitudes above 20°N. Figure 13a shows strong southwesterly CO fluxes over southern China from 20°N and 30°N, which results from the collocation of high emissions with the convergence zone. This convergence results in an upward flux of CO, which lifts the pollution above the boundary layer into the free atmosphere where it is caught by the strong westerlies. We thus find that the strongest export of CO from the Asia continent to the western Pacific is at 2~6 km even through the highest concentrations are found in the lower atmosphere below 2 km (Figures 14a and 14b).

CO from biomass burning sources, mainly emitted in Southeast Asia, is transported towards the convergence zone over the continent by anticyclonic circulation over Southeast Asia. Over the convergence zone it is uplifted into the free troposphere and then is carried by the strong westerlies. Figure 14b shows that large amounts of CO from biomass burning are exported in the free troposphere, contributing more than 35%

to the CO peak fluxes. Little biomass CO is exported in the boundary layer. Substantial export of CO from fuel combustion is found in the boundary layer by the monsoon winds, especially at latitudes higher than 35°N.

Figure 13b shows two zones (20-33°N and 38-50°N) of strong southwesterly O_3 fluxes. These vertically integrated horizontal fluxes in the lower troposphere (0 ~ 2.5 km) focus on export of photochemically produced O_3. High O_3 concentrations in the boundary layer are seen in Figure 8 in Southeast Asia, southern and eastern China and over the western Pacific at middle latitudes. Elevated ozone is the result of significant photochemical production and preferential transport towards the east and northeast due to the prevailing atmospheric circulation during this period. In the upper free troposphere O_3 mixing ratios are under strong influence of stratospheric ozone at latitudes above 20°N. Figure 14c shows high O_3 concentrations in the lower troposphere in the middle latitudes and in the upper troposphere; a feature that is very similar to the observed average latitudinal distributions [*Browell et al., this issue*] south of 39°N. Strong O_3 export in the middle latitudes mainly results from high photochemical production and the convergence zone described above; and the large flux at the high latitudes is due to the influence of a larger downward flux from the stratosphere and strong monsoon winds.

There are two zones of high SO_4^{2-} fluxes (Figure 13c). One in the middle latitudes is related to anthropogenic sources, and the other is associated with the Miyakejima volcano emissions. We see high SO_4^{2-} fluxes in the area just downwind of the volcano. Figure 14f shows that the strongest export flux of SO_4^{2-} to the western Pacific is at ~2 km altitude even through the highest concentrations are found below ~1 km altitude (Figure 14e), due to the convergence zone described previously.

2.2. Process Analysis

The AVHRR satellite images show that considerable biomass burning took place in Southeast Asia and southern China during the study period, and the model results indicate that biomass burning emissions strongly influence the overall CO and O_3 distributions. Biomass burning contributes more than 50% of the CO concentrations in the boundary layer over the major source regions while indirectly contributing up to 40% of the O_3 concentrations (Figures 7 and 8). The largest percentage contributions of biomass burning to CO and O_3 levels over the western Pacific are found in the lower free troposphere. For illustrating the impacts of biomass burning emissions, as well as various transport and chemical processes, a processes analysis was performed. The atmospheric chemistry and its contributions to Asian outflow, the sources and sinks of CO, O_3, NO_x, HNO_3, PAN, SO_2 and SO_4^{2-} in the whole model domain below 9 km in two simulations with (base) and without (test) biomass burning emissions during the study period are summarized in Table 2. In the table TRT includes the contributions from transport and diffusion processes. CHEM stands for the gas-phase chemical production, AQUE accounts for the impacts of aqueous chemistry and cloud processes, EMIS represents emissions,

and DEP is the sum of dry and wet deposition. Negative values indicate the mass of the species decreased by this process.

Table 2 shows that CO emissions from biomass burning are higher than its regional anthropogenic sources, and most of the CO emitted in East Asia is transported out of the domain. From the table we find that photochemically produced O_3 in the base case is two times more than in the test case, which means biomass burning increases O_3 photochemical production by more than 50%. The increase in ozone production, also results in an increase in ozone export and dry and wet deposition, as shown in the table.

Table 2 also shows that about 26% of NO_x emissions come from biomass burning. Because of the short lifetime of NO_x, most NO_x emitted in the sampled domain is converted to HNO_3 and PAN, and biomass burning increases their chemical production (the difference in chemical production between base and test cases divided by chemical production in base case) by ~32% and ~30%, respectively. Because HNO_3 is quickly removed by dry and wet (including cloud processes and aqueous chemistry) deposition, only ~20% (TRT divided by CHEM) of HNO_3 produced in the base case is exported outside of the sampled domain, while ~90% of PAN is exported.

In the table the budgets for SO_2 and SO_4^{2-} clearly show the conversion pathway of SO_2 to SO_4^{2-} in the study period. In the base case, ~43% (the sum of AQUE and CHEM divided by EMIS) SO_2 emitted is oxidized, ~25% deposited by dry and wet removal processes, and ~24% transported out of the domain. From the SO_4^{2-} budget we see that the aqueous-phase conversion of SO_2 to SO_4^{2-} contributes more than 61% (AQUE divided by the sum of AQUE and CHEM) to the total SO_4^{2-} production, and ~29% (TRT divided by the sum of AQUE, CHEM and EMIS) of SO_4^{2-} is transported out of the domain.

As the rate of SO_2 oxidation rate is determined by the reaction of SO_2 with hydroxyl radical (OH) in the gas-phase, and with hydrogen peroxide (H_2O_2) and O_3 in the aqueous-phase, and the emissions from biomass burning increase O_3 and H_2O_2 mixing ratios, biomass burning increases the SO_2 oxidation rate, and consequently will increase SO_4^{2-} production rate. Table 2 shows that the total amount of SO_4^{2-} produced in the base case is larger than in the test case, but the difference between them is small due to the fact that biomass burning mainly occurs in Southeast Asia and southern China, while the major SO_2 sources are in eastern and northeastern China and Seoul area of South Korea.

4. Summary

We utilized the Models-3 Community Multi-scale Air Quality modeling system (CMAQ) with meteorological fields from the Regional Atmospheric Modeling System (RAMS) to examine the Asian outflow of CO, O_3 and SO_4^{2-} over the western Pacific during the period of March 17 to 24, 2001. Considerable biomass burning took place in Southeast Asia and southern China during this time, and these fires were estimated to cause emissions of CO and NO_x that are of comparable magnitudes to the regional anthropogenic sources. Comparisons of the model results with the TRACE-P observations for CO, O_3 and SO_4^{2-} showed that the model

reproduces well the latitudinal and vertical distribution of the pollutants in the Asian outflow with the highest concentrations found below 3 km altitude and north of 25°N.

Analysis of model results revealed that the fast boundary layer outflow from Asia to the western Pacific is largely restricted to the middle latitudes. Although observations and simulations indicate the highest outflow concentrations over the western Pacific are in the lower troposphere (0-3 km), the maximum outflow fluxes are predicted to be in the free troposphere (3-6 km), reflecting episodic uplifting of pollution over central and eastern China into the free troposphere and the stronger westerlies. The convergence zone in central and eastern China is shown to be of particular importance for driving the outflow of biomass burning emissions in Southeast Asia and Southern China. A budget analysis showed that the emissions from biomass burning have an important influence on atmospheric chemistry in Asia. Biomass burning is found to contribute more than 50% of the CO concentrations and up to 40% of the O_3 concentrations in the boundary layer over the major source regions. The largest percentage contributions to CO and O_3 levels (up to 40% and 30% respectively) over the western Pacific are estimated to be in the lower free troposphere (2-6 km).

Finally these results help to illustrate the complex nature of Asian outflow in the spring, and how fuel and open burning emissions from East and Southeast Asia, can become intertwined. Further work is needed to more completely understand and resolve the complex vertical structures in the lower marine troposphere. High-resolution modeling studies are being performed for this period and will be the subject of a future paper.

Acknowledgments. This work was partly supported by Research and Development Applying Advanced Computational Science and Technology (ACT-JST), CREST of Japan Science and Technology Corporation and National Natural Science Foundation of China (project number: 40245029). This work was also supported in part by grants from the NASA ACMAP and GTE programs, the NSF Atmospheric Chemistry Program, and Hundred Talents Program (Global Environmental Change) from Chinese Academy of Sciences.

We also want to thank National Institute for Environmental Studies (NIES) of Japan for O_3 observational data at the Ochiishi and Hateruma stations in Japan, and C. Harward (SAIC Inc.) and T. Slate (Swales Inc.) for observational data.

References

Beekmann, M., G. Ancellet, and G. Megie, Climatology of tropospheric ozone in southern Europe and its relation to potential vorticity, *J. Geophys. Res.,* **99**, 12,841-12,853, 1994.

Benkovitz, C.M., M.T. Schultz, J. Pacyna, L. Tarrason, J. Dignon, E.C. Voldner, P.A. Spiro, J.A. Logan, and T.E. Graedel, Global gridded inventories of anthropogenic emissions of sulfur and nitrogen, *J. Geophys. Res.,* **101**, 29,239-29,253, 1996.

Berntsen, T., I.S.A. Isaksen, W.C. Wang, and X.Z. Liang, Impacts of increased anthropogenic emissions in Asia on thropospheric ozone and climate – A global 3-D model study, *Tellus,* **48**, 13-32, 1996.

Berntsen, T.K., S. Karlsdottir, and D.A. Jaffe, Influence of Asian emissions on the composition of air reaching the North Western United States, *Geophys. Res. Lett.,* **26**, 2171-2174, 1999.

Binkowski, F.S., and U. Shankar, The regional particulate matter model: 1. Model description and preliminary results, *J. Geophys. Res.,* **100**, 26,191-26,209, 1995.

Browell, et al., Large-scale air mass characterization observed over the western Pacific during the TRACE-P, *J. Geophys. Res.,* (this issue).

Byun, D.W., and J.K.S. Ching, ed., *Science algorithms of the EPA Models-3 community multi-scale air quality (CMAQ) modeling system*, NERL, Research Triangle Park, NC, 1999.

Byun, D.W., Dynamically consistent formulation in meteorological and air quality models for multiscale atmospheric studies. Part II: Mass conservation issues, *J. Atmos. Sci.,* **56**, 3808-3820.

Carmichael, G.R., I. Uno, M.J. Phadnis, Y. Zhang, and Y. Sunwoo, Tropospheric ozone production and transport in the springtime in east Asia, *J. Geophys. Res.,* **103**, 10,649-10,671, 1998.

Carmichael, R.A., Y. Tang, G. Kurata, I. Uno, D. Streets, J. Woo, H. Huang, J. Yienger, B. Lefer, R.E. Shetter, D.R. Blake, G. Sacshe, M. Avery, A. Clarke, N. Thongboonchoo, Regional-scale chemical transport modeling in support of intensive field experiments: Overview and analysis of the TRACE-P observations, *J. Geophys. Res.,* (this issue).

Carter, W.P.L., Condensed atmospheric photooxidation mechanisms for isoprene, *Atmos. Environ.,* **24**, 4,275-4,290, 1996.

Christopher, D.E., J. Chou, R.M. Welch, D.V. Kliche and V.S. Connors, Satellite investigations of fire, smoke, and carbon monoxide during April 1994 MAPS mission: Case studies over tropical Asia, *J. Geophys. Res.*, **103**, 19,327-19,336, 1998.

Colella, P., and P.L. Woodward, The piecewise parabolic method (PPM) for gas-dynamical simulations, *J. Comp. Phys.,* **54**, 174-201, 1984.

Crawford, J., et al., An assessment of ozone photochemistry in the extratropical western North Pacific: Impact of continental outflow during the late winter/early spring, *J. Geophys. Res.,* **102**, 28,469-28,487, 1997.

Crutzen, P.J. and M.O. Andreae, Biomass burning in the tropics: impact on atmospheric chemistry and biogeochemical cycles. *Science,* **250**, 1669-1678, 1990.

Dentener, F. J., G. R. Carmichael, Y. Zhang, J. Lelieveld, and P. J. Crutzen, Role of mineral aerosol as a reactive surface in the global troposphere, *J. Geophys. Res*, **101**, 22,869-22,889, 1996.

Ebel, A., H. Hass, H. Jacobs, M. Laube, M. Memmesheimer, and A. Oberreuter, Simulation of ozone intrusion caused by tropopause fold and cut-off low, *Atmos. Environ.,* **25(A)**, 2131-2144, 1991.

Galanter, M., H. II Levy, and G.R. Carmichael, Impacts of biomass burning on tropospheric CO, NO_x and O_3, *J. Geophys. Res.,* **105**, 6633-6653, 2000.

Jaffe, D., A. Mahura, J. Kelly, J. Atkins, P.C. Novelli, and J.T. Merrill, Impacts of Asian emissions on the remote North Pacific atmosphere: Interpretation of CO data from Shemya, Guam, Midway, amd Mauna Loa, *J. Geophys. Res.,* **102**, 28,627-28,635, 1997.

Jaffe, D.A., et al., Transport of Asian air pollution to North America, *Geophys. Res. Lett.,* **26**, 711-714, 1999.

Kato, N., and H. Akimoto, Anthropogenic emissions of SO_2 and NO_x in Asia: Emission inventories, *Atmos. Environ., Part A,* **26**, 2997-3017, 1992.

Lee, T.J., The impact of vegetation on the atmospheric boundary layer and convective storms. Atmospheric Science Paper No. 509, Dept. of Atmos. Sci., Colorado State Univ., Fort Collins, CO., 1992.

Liu, H., W.L. Chang, S.J. Oltmans, L.Y. Chan, and J.M. Harisse, On springtime high ozone events in the lower troposphere from Southeast Asia biomass burning, *Atmos. Environ.,* **33**, 2403-2410, 1999.

Liu, S.C., et al., Model study of tropospheric trace species distributions during PEM-West A, *J. Geophys. Res.,* **101**, 2073-2085, 1996.

Louis, J.-F., A parametric model of vertical eddy fluxes in the atmosphere, *Boundary-Layer Meteorol.,* **17**, 187-202, 1979.

Mauzerall, D.L., D. Narita, H. Akimoto, L. Horowitz, S. Walters, D. Hauglustaine, and G. Brasseur, Seasonal characteristics of tropospheric ozone production and mixing ratios over East Asia:

A global three-dimensional chemical transport analysis, *J. Geophys. Res.,* **105**, 17895-17910, 2000.

Mellor, G.L., and T. Yamata, A hierachy of turbulence closure models for planetary boundary layers, *J. Atmos. Sci.,* **31**, 1791-1806, 1974.

Nguyen, B., N. Mihalopoulos, and J.-P. Putaud, Rice straw burning in Southeast Asia as a source of CO and COS to the atmosphere, *J. Geophys. Res.,* **99**, 16,435-16,439, 1994.

Oliver, J.G.J., et al., Description of EDGAR Version 2.0: *A set of global emission inventories of greenhouse gases and ozone-depleting substances for all anthropogenic and most natural sources on a per country basis and on 1^0x1^0 grid,* National Institute of Public Health and the Environment (RIVM) report no. 771060 002 / TNO-MEP report no. R96/119, 1996.

Pielke, R.A., W.R. Cotton, R.L. Walko, C.J. Tremback, W.A. Lyons, L.D. Grasso, M.E. Nicholls, M.D. Moran, D.A. Wesley, T.J. Lee and J.H. Copeland, A comprehensive meteorological modeling system – RAMS, *Meteorol. Atmos. Phys.*, **49**, 69-91, 1992.

Song, C.-H., and G.R., Carmichael, A three-dimensional modeling investigation of the evolution processes of dust and sea-salt particles in east Asia, *J. Geophys. Res*, **106**, 18,131-18,154, 2001.

Stockwell, W.R., P. Middleton and J.S. Chang, The second generation regional acid deposition model chemical mechanism for regional air quality modeling, *J. Geophy. Res.,* **95**, 16,343-16,367, 1990.

Streets, D.G., T.C. Bond, G.R. Carmichael, S. Fermandes, Q. Fu, D. He, Z. Klimont, S.M. Nelson, N.Y. Tsai, M.Q. Wang, J.-H. Woo, and K.F. Yarber, A inventory of gaseous and primary aerosol emissions in Asia in the year 2000, *J. Geophys. Res.,* (this issue).

Talbot, R. W., et al., Chemical characteristics of continental outflow from Asia to the troposphere over the western Pacific Ocean during February – March 1994: Results from PEM-West B, *J. Geophys. Res.,* **102**, 28255-28274, 1997.

Tang, Y, et al., The influence of biomass burning during TRACE-P experiment identified by the regional chemical transport model, *J. Geophys. Res.,* (this issue).

Tu, F., D. Thornton, A. Bandy, M. Kim, G. Carmichael, Y. Tang, L. Thornhill, and G. Sachse, Dynamics and transport of SO2 over the Yellow Sea dueing Trcae-P, *J. Geophys. Res.,* (this issue).

Uematsu, M., R.A. Duce, J.M. Prospero, L. Chen, J.T. Merrill, and R.L. McDonald, Transport of mineral aerosol from Asia over the North Pacific Ocean, *J. Geophys. Res.,* **88**, 5343-5352, 1983.

Uno, I, X.-M. Cai, D.G. Steyn and S. Emori, A simple extension of Louis method for rough surface layer modeling, *Boundary-Layer Meteorol.,* **76**, 395-405, 1995.

Uno, I., H. Amano, S. Emori, K. Kinoshita, I. Matsui and N. Sugimoto: Trans-Pacific Yellow Sand Transport observed in April 1998: Numerical Simulation, *J. Geophy. Res.*, **106**, 18,331-18,344, 2001.

Van Aardenne, J.A., G.R. Carmichael, H. Levy II, D. Streets, and L. Hordjik, Anthropogenic NO_x emissions in Asia in the period 1990-2020, *Atmos. Environ.,* **33**, 633-646, 1999.

Walko, R.L., W.R. Cotton, M.P. Meyers, and J.Y. Harrington, New RAMS cloud microphysics parameterization, part I: the single-moment sheme, *Atmospheric Research*, **28**, 29-62, 1995.

Wang, Z., H. Ueda and M. Huang, A deflation module for use in modeling long-range transport of yellow sand over East Asia, *J. Geophys. Res,* **105**, 26,947-26,960, 2000.

Wang. Y., D.J. Jacob and J.A. Logan, Global simulation of tropospheric O3-NOx-hydrocarbon chemistry. 1. Model formulation. *J. Geophy. Res.*, **103**, 10,713-10,725, 1998.

Woo, J., Y. Tang, D.G. Streets, J. Dorwart, G.R. Carmichael, S. Pinnock, K.F. Yarber, G. Kurata, and N. Thongboonchoo, Biomass and biogenic emissions and their impact on trace gas distribution during TRACE-P, *J. Geophys. Res.,* (this issue).

Yienger, J.J., M. Galanter, T.A. Holloway, M.J. Phadnis, S.H. Guttikunda, G.R. Carmichael, W.J. Moxim, and H. Levy II, The episodic nature of air pollution transport from Asia to North America, *J. Geophys. Res.,* **105**, 26,931-26,945, 2000.

Zhang, M., I. Uno, S. Sugata, Z. Wang, D. Byun, and H. Akimoto, Numerical study of boundary layer ozone transport and

photochemical production in east Asia in the wintertime, *Geophys. Res. Lett*., 10.1029/2001GL014368, 2002.

Zhang, Y., and G.R. Carmichael, The role of mineral aerosol in tropospheric chemistry in East Asia – A model study, *J. Appl. Meteorol.,* **38**, 353-366, 1999.

H. Akimoto, Frontier Research System for Global Change, Yokohama, Kanagawa 236-0001, Japan. (e-mail: akimoto@jamstec.go.jp)

I. Uno, Research Institute for Applied Mechanics of Kyushu University, Kasuga Park 6-1, Kasuga 816-8580, Japan. (e-mail: iuno@riam.kyushu-u.ac.jp)

Z. Wang and M. Zhang (corresponding author), State Key Laboratory of Atmospheric Boundary Layer Physics and Atmospheric Chemistry, Institute of Atmospheric Physics, Chinese Academy of Sciences, Beijing, China. (e-mail: zifawang@mail.iap.ac.cn; mgzhang@mail.iap.ac.cn)

ZHANG ET AL.: TRACE GASES AND AEROSOLS DURING TRACE-P
ZHANG ET AL.: TRACE GASES AND AEROSOLS DURING TRACE-P
ZHANG ET AL.: TRACE GASES AND AEROSOLS DURING TRACE-P
ZHANG ET AL.: TRACE GASES AND AEROSOLS DURING TRACE-P
ZHANG ET AL.: TRACE GASES AND AEROSOLS DURING TRACE-P
ZHANG ET AL.: TRACE GASES AND AEROSOLS DURING TRACE-P
ZHANG ET AL.: TRACE GASES AND AEROSOLS DURING TRACE-P
ZHANG ET AL.: TRACE GASES AND AEROSOLS DURING TRACE-P
ZHANG ET AL.: TRACE GASES AND AEROSOLS DURING TRACE-P
ZHANG ET AL.: TRACE GASES AND AEROSOLS DURING TRACE-P
ZHANG ET AL.: TRACE GASES AND AEROSOLS DURING TRACE-P
ZHANG ET AL.: TRACE GASES AND AEROSOLS DURING TRACE-P
ZHANG ET AL.: TRACE GASES AND AEROSOLS DURING TRACE-P
ZHANG ET AL.: TRACE GASES AND AEROSOLS DURING TRACE-P
ZHANG ET AL.: TRACE GASES AND AEROSOLS DURING TRACE-P
ZHANG ET AL.: TRACE GASES AND AEROSOLS DURING TRACE-P
ZHANG ET AL.: TRACE GASES AND AEROSOLS DURING TRACE-P
ZHANG ET AL.: TRACE GASES AND AEROSOLS DURING TRACE-P
ZHANG ET AL.: TRACE GASES AND AEROSOLS DURING TRACE-P
ZHANG ET AL.: TRACE GASES AND AEROSOLS DURING TRACE-P
ZHANG ET AL.: TRACE GASES AND AEROSOLS DURING TRACE-P
ZHANG ET AL.: TRACE GASES AND AEROSOLS DURING TRACE-P
ZHANG ET AL.: TRACE GASES AND AEROSOLS DURING TRACE-P
ZHANG ET AL.: TRACE GASES AND AEROSOLS DURING TRACE-P
ZHANG ET AL.: TRACE GASES AND AEROSOLS DURING TRACE-P
ZHANG ET AL.: TRACE GASES AND AEROSOLS DURING TRACE-P
ZHANG ET AL.: TRACE GASES AND AEROSOLS DURING TRACE-P
ZHANG ET AL.: TRACE GASES AND AEROSOLS DURING TRACE-P

Figure 1. Model domain for RAMS (outer region) and CMAQ (inside region) used in this study. Also shown are the locations of the observation sites at Ochiishi and Hateruma. The thick solid line indicates the transect at which mass fluxes are estimated.

Figure 2. The horizontal DC-8 (red line) and P-3B (blue line) flight tracks in the study period. Numbers are flight time in JST (Japanese Standard Time), and symbols in green designate specific features discussed in the text.

Figure 3. Time series of observed (closed circle, ppbv) and simulated concentrations of CO with (triangle, ppbv) and without (open circle, ppbv) biomass burning emissions along the flight tracks (dashed line, km). Also shown in (a), (c), (e), and (g) are CO concentrations (solid line, ppbv) predicted by the Sulfur Transport Eulerian Model (STEM) as discussed in *Carmichael et al.* [this issue]. Letters designate the flight segments identified in Figure 2.

Figure 4. Time series of observed (closed circle, ppbv) and simulated concentrations of O_3 with (triangle, ppbv) and without (open circle, ppbv) biomass burning emissions along the flight tracks (dashed line, km). Letters designate the flight segments identified in Figure 2.

Figure 5. Time series of observed (closed circle, ug/m^3) and simulated (triangle, ug/m^3) concentrations of SO_4^{2-} along the flight tracks (dashed line, km). Letters designate the flight segments identified in Figure 2.

Figure 6. Comparison between modeled hourly average ozone mixing ratios (solid line, ppbv) for the lowest model (~150 m above ground) and observed ground level hourly mean ozone concentrations (dots, ppbv) in March of 2001 at (a) Ochiishi and (b) Hateruma.

Figure 7. Horizontal distributions of average CO concentrations (shaded, ppbv) and the percentage contributions (contour with intervals 10, %) from biomass burning in the boundary layer (from surface to 1000 m) at 0300 Z (1200 JST) on March 17, 18, 20, 21, 23 and 24, 2001.

Figure 8. Horizontal distributions of average O_3 concentrations (shaded, ppbv) and the percentage contributions (contour with intervals 10, %) from biomass burning in the boundary layer (from surface to 1000 m) at 0300 Z (1200 JST) on March 17, 18, 20, 21, 23 and 24, 2001.

Figure 9. Horizontal distributions of average SO_4^{2-} concentrations (ug/m^3) in the boundary layer (from surface to 1000 m) at 0300 Z (1200 JST) on March 17, 18, 20, 21, 23 and 24, 2001. Also shown are wind vectors at an altitude of ~500 m.

Figure 10. Vertical distributions of CO concentrations (ppbv, shaded) and the percentage contributions (%, contour) from biomass burning along the DC-8 flight tracks.

Figure 11. Vertical distributions of O_3 concentrations (ppbv, shaded) and the percentage contributions (%, contour) from biomass burning along the DC-8 flight tracks.

Figure 12. Vertical distributions of SO_4^{2-} concentrations (ug/m^3) along the DC-8 flight tracks.

Figure 13. Average horizontal fluxes of (a) CO (10^{-5} mole/m^2/s), (b) O_3 (10^{-5} mole/m^2/s) and SO_4^{2-} (10^{-7} mole/m^2/s) and their magnitudes (shaded) vertically integrated from surface to 9 km except for O_3 to 2.5 km in the period March 17-24, 2001.

Figure 14. Average concentrations of (a) CO (ppbv), (c) O3 (ppbv) and (e) SO_4^{2-} (ug/m^3) and zonal fluxes of (b) CO (shaded, 10^{-5}mole/m^2/s) and (d) O_3 (shaded, 10^{-5}mole/m^2/s) with their percentage contributions from biomass burning (contour, %) and (f) SO_4^{2-} (shaded, 10^{-7}mole/m^2/s) in the period March 17-24, 2001, along 125^{o}E.

Table 1. Emissions in March of 2001 used in this study

	China	Japan	SE+India	Model domain
CO	51.77 (13.42)	2.13	63.91 (55.47)	132.34 (73.13)
NO_x (10^{11} g N)	2.50 (0.26)	0.57	1.51 (1.04)	6.04 (1.38)
SO_2 (10^{11} g S)	9.26	3.97	0.67	16.84
Ethane	1.81 (0.10)	0.15	0.88 (0.41)	3.26 (0.54)
Propane	2.21 (0.04)	0.30	0.58 (0.17)	4.06 (0.22)
Ethene	1.73	0.15	0.98	3.71
Terminal olefins	1.27 (0.29)	0.07	1.82 (1.18)	3.56 (1.56)
Internal olefins	0.73 (0.29)	0.07	2.69 (1.19)	3.97 (1.56)
Toluene and less reactive aromatics	0.89	0.11	0.54	1.86
Xylene and more reactive aromatics	0.39	0.13	0.17	0.91
Formaldehyde	0.07	0.01	0.05	0.15
Acetaldehyde and higher aldehydes	0.15 (0.01)	0.01	0.15 (0.05)	0.36 (0.07)
Isoprene	2.11	0.07	19.42	24.60

[1)]Values in the brackets are contributions from biomass burning emissions.
[2)]Unit for CO and hydrocarbons are in 10^{11} g C.
[3)]In Japan anthropogenic SO_2 emissions were 0.52×10^{11} g S, while the Miyakejima volcano emitted 3.30×10^{11} g S.
[4)]SE+India covers Southeast Asia and part of India.

Table 2. Sources and sinks of CO, O_3, NO_x, HNO_3, PAN, SO_2 and SO_4^{2-} in the whole model domain below 9km ($6240 \times 5440 \times 9$ km^3) in the period March 17-24, 2001 (Unit: 10^8 mole)

		TRT*	CHEM*	AQUE*	EMIS*	DEP*
CO (x100)**	Base	-23.7	-4.5	-1.8	32.9	
	Test	-9.6	-1.0	-0.7	13.2	
O_3 (x10)**	Base	-116.9	80.1	41.4		-36.9
	Test	-82.8	35.2	43.3		-33.2
NO_x	Base	1.2	-121.0	-0.4	121.8	-1.7
	Test	2.2	-90.6	-0.1	90.0	-1.5
HNO_3	Base	-32.2	157.5	-64.2		-37.0
	Test	-20.4	107.5	-42.1		-28.7
PAN	Base	-40.7	45.3	-1.3		
	Test	-29.0	31.6	-0.5		
SO_2	Base	-33.3	-26.0	-35.0	141.5	-35.7
	Test	-33.7	-25.4	-34.8	141.5	-36.0
SO_4^{2-}	Base	-21.2	25.2***	40.2	7.1****	-38.5
	Test	-21.0	24.5***	40.0	7.1****	-38.0

*In the table TRT includes the contributions from transport and diffusion processes, CHEM stands for the gas-phase chemical production, AQUE accounts for the impacts of aqueous chemistry and cloud processes, EMIS represents emissions, and DEP is the sum of dry and wet deposition. Negative values indicate the mass of the species decreased by this processes.
**Values for CO and O_3 budgets are 100 and 10 times larger than shown.
***It represents the net production of SO_4^{2-} related to the processes of SO_2 oxidation via the gas-phase chemistry.
****In this study it is assumed that 5% of SO_2 emitted was in the form of H_2SO_4, while H_2SO_4 is fast converted to SO_4^{2-}, so H_2SO_4 is treated as the direct emission of SO_4^{2-} here.

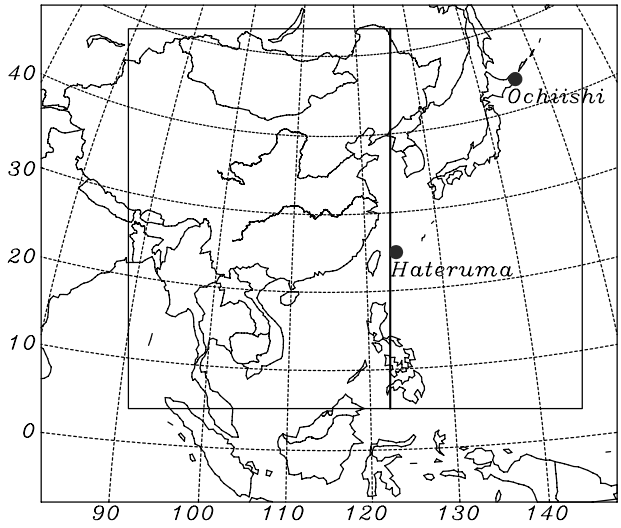

Figure 1. Model domain for RAMS (outer region) and CMAQ (inside region) used in this study. Also shown are the locations of the observation sites Ochiishi and Hateruma. The thick solid line indicates the transect at which mass fluxes are estimated

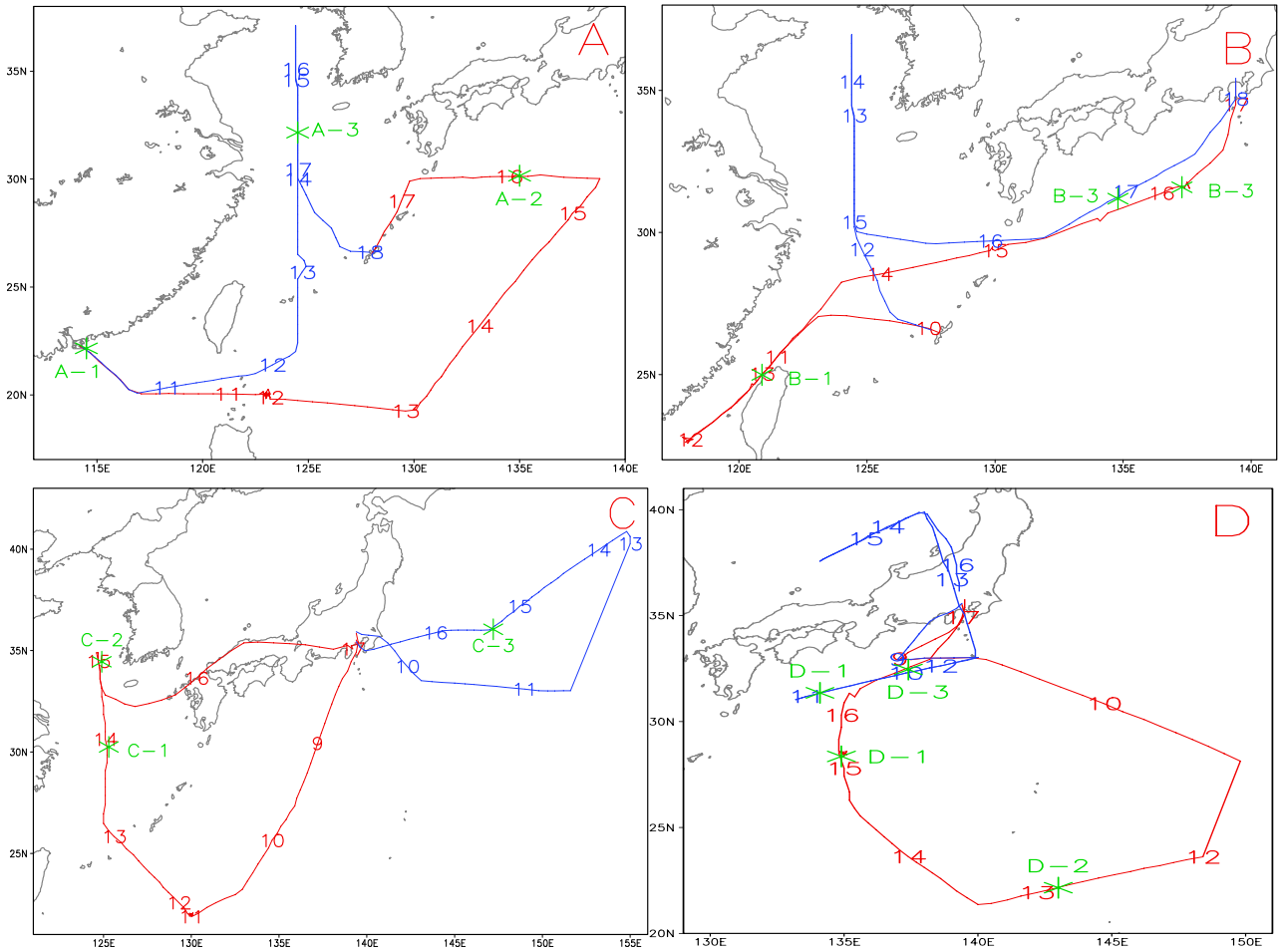

Figure 2. The horizontal DC-8 (red line) and P-3B (blue line) flight tracks in the study period. Numbers are flight time in JST (Japanese Standard Time), and symbols in green designate specific features discussed in the text.

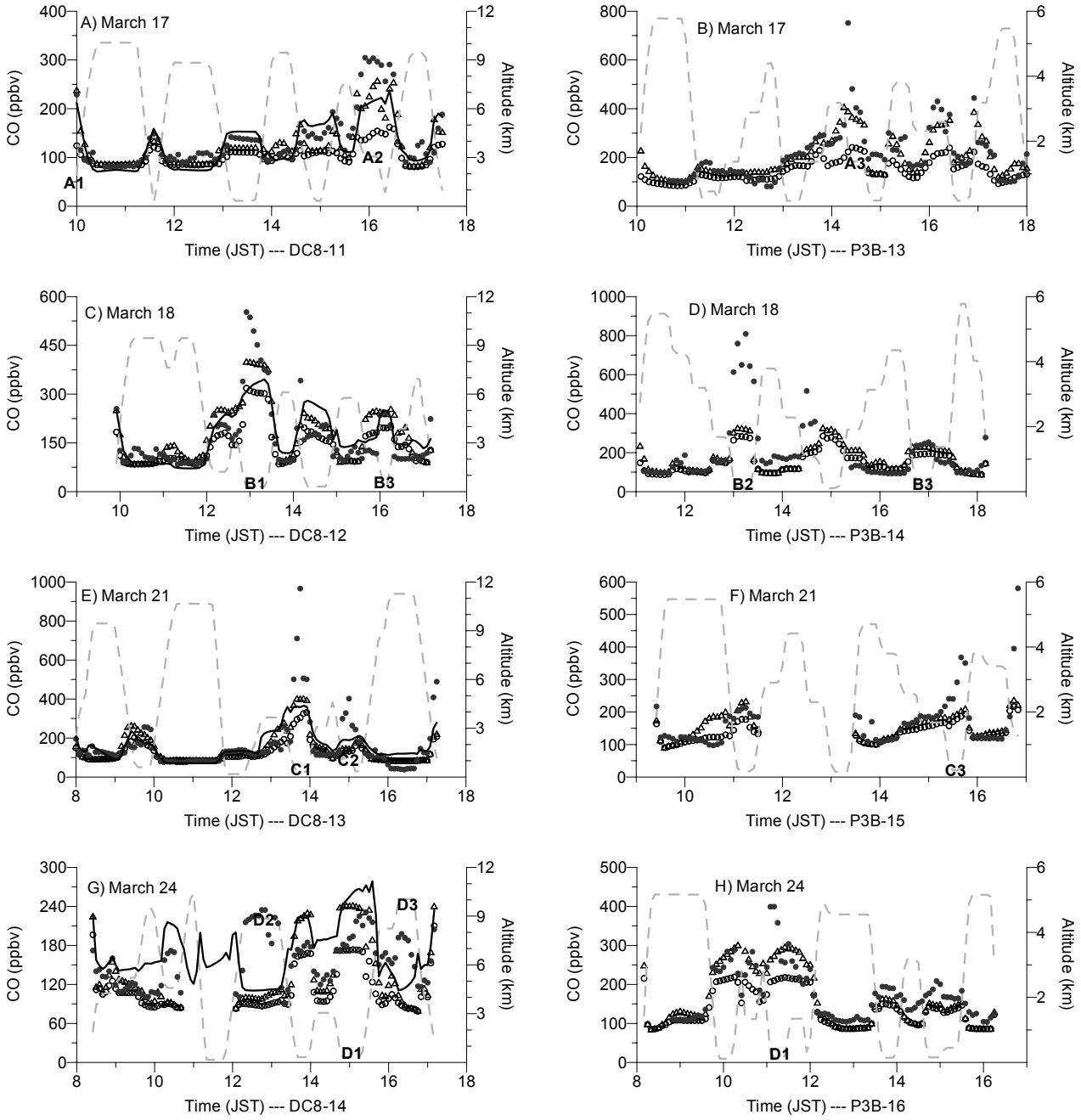

Figure 3. Time series of observed (closed circle, ppbv) and simulated concentrations of CO with (triangle, ppbv) and without (open circle, ppbv) biomass burning emissions along the flight tracks (dashed line, km). Also shown in (a), (c), (e) and (g) are CO concentrations (solid line, ppbv) predicted by use of the Sulfur Transport Eulerian Model (STEM) as discussed in *Carmichael et al.* [this issue]. Letters designate the flight segments identified in Figure 2.

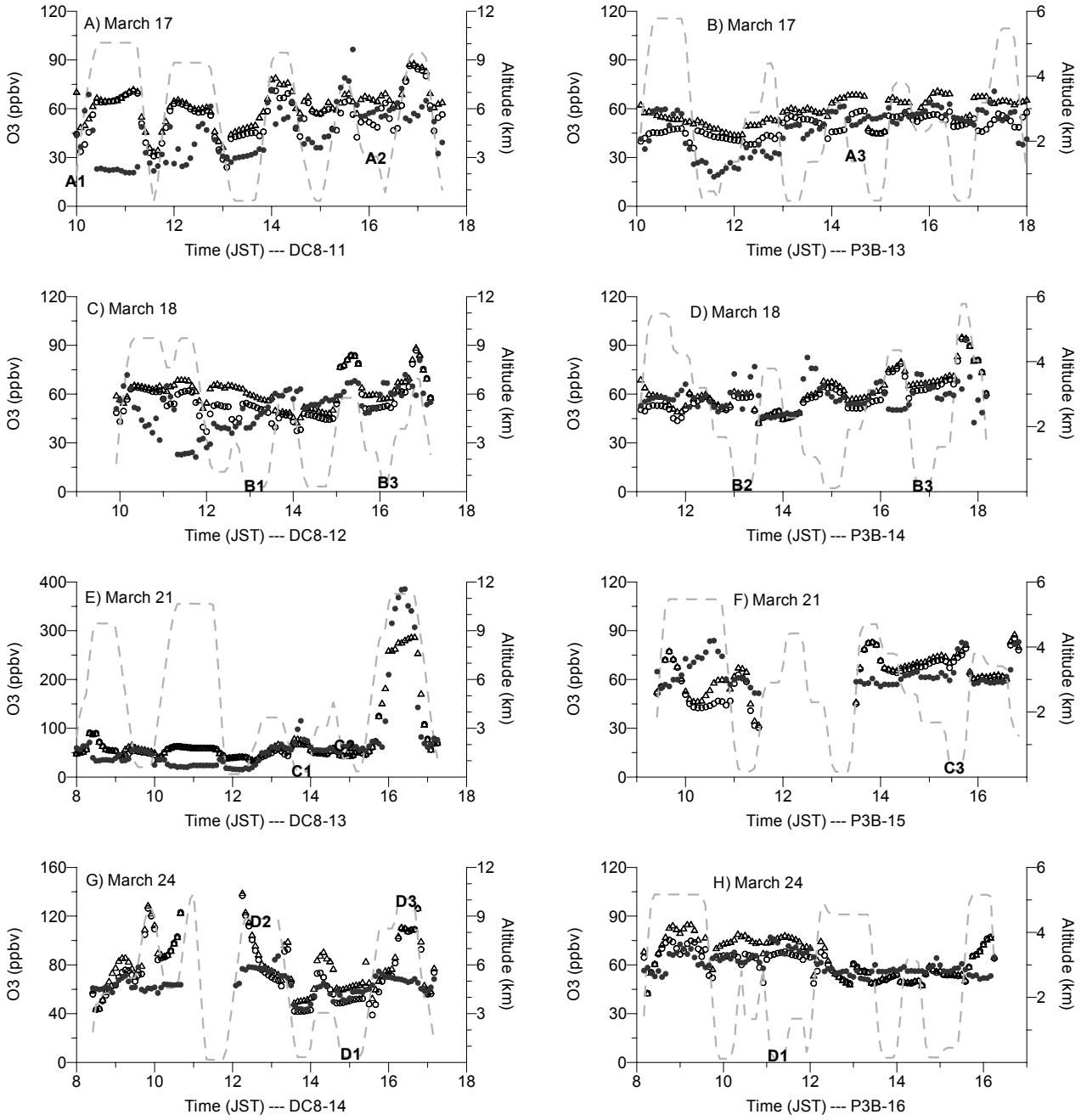

Figure 4. Time series of observed (closed circle, ppbv) and simulated concentrations of O_3 with (triangle, ppbv) and without (open circle, ppbv) biomass burning emissions along the flight tracks (dashed line, km). Letters designate the flight segments identified in Figure 2.

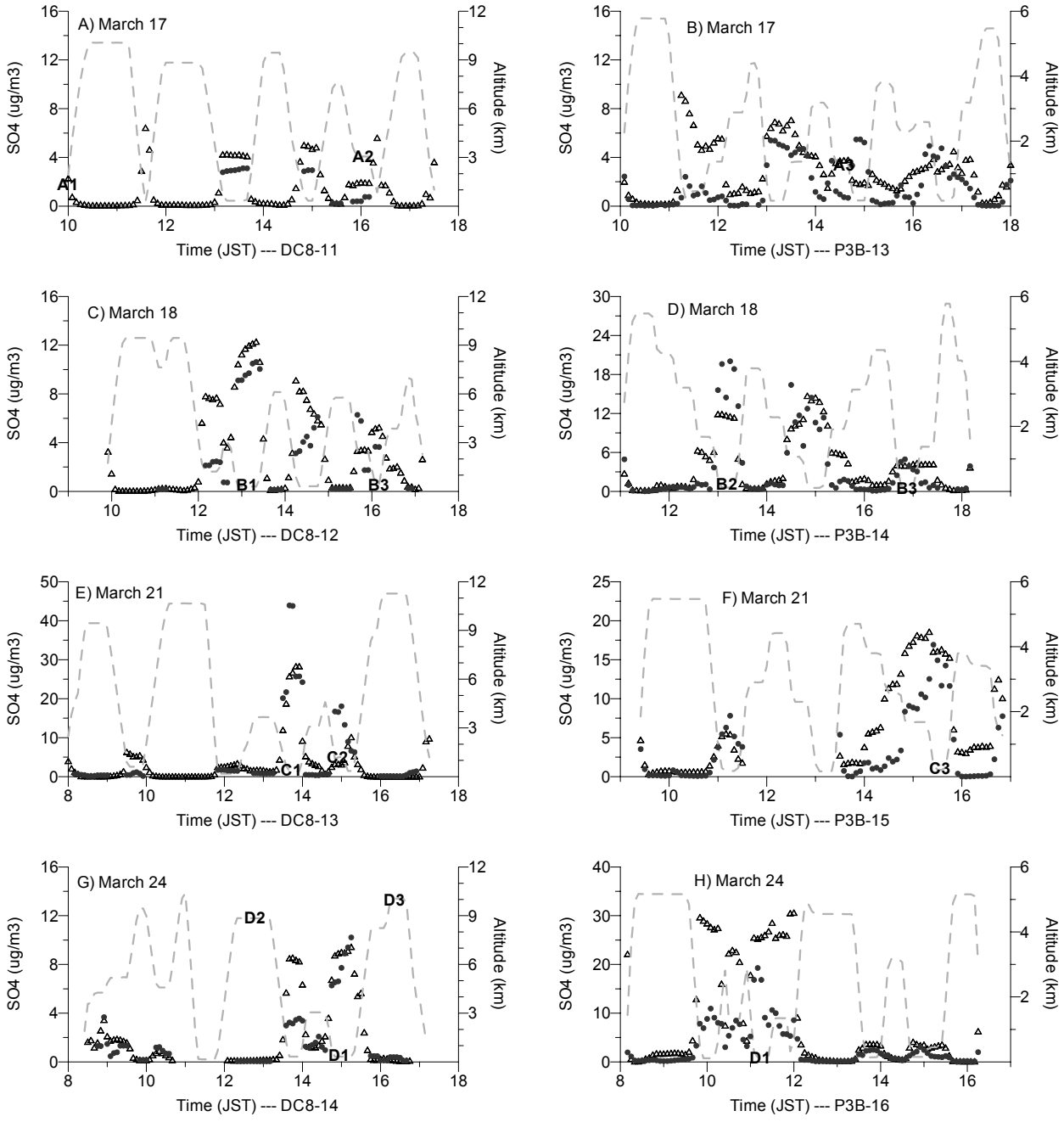

Figure 5. Time series of observed (closed circle, ug/m^3) and simulated (triangle, ug/m^3) concentrations of SO_4^{2-} along the flight tracks (dashed line, km). Letters designate the flight segments identified in Figure 2.

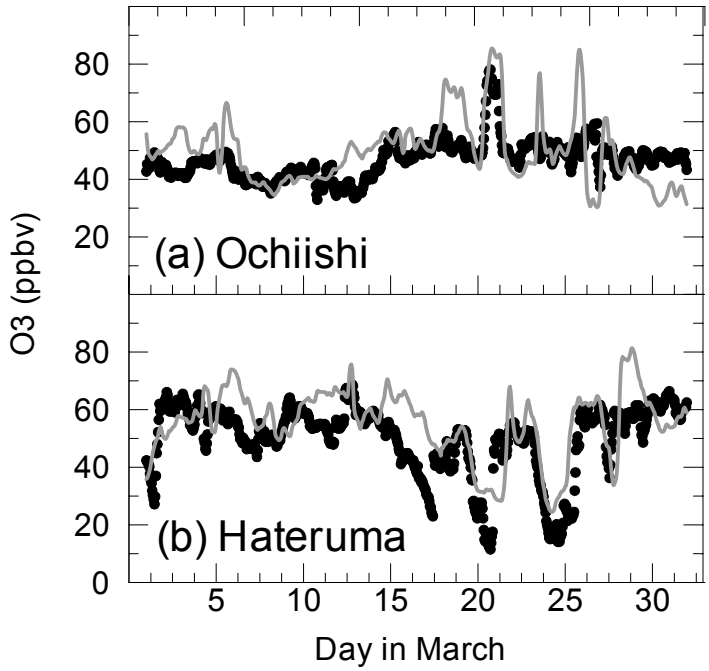

Figure 6. Comparison between modeled hourly average ozone mixing ratios (solid line, ppbv) for the lowest model (~150 m above ground) and observed ground level hourly mean ozone concentrations (dots, ppbv) in March of 2001 at (a) Ochiishi and (b) Hateruma.

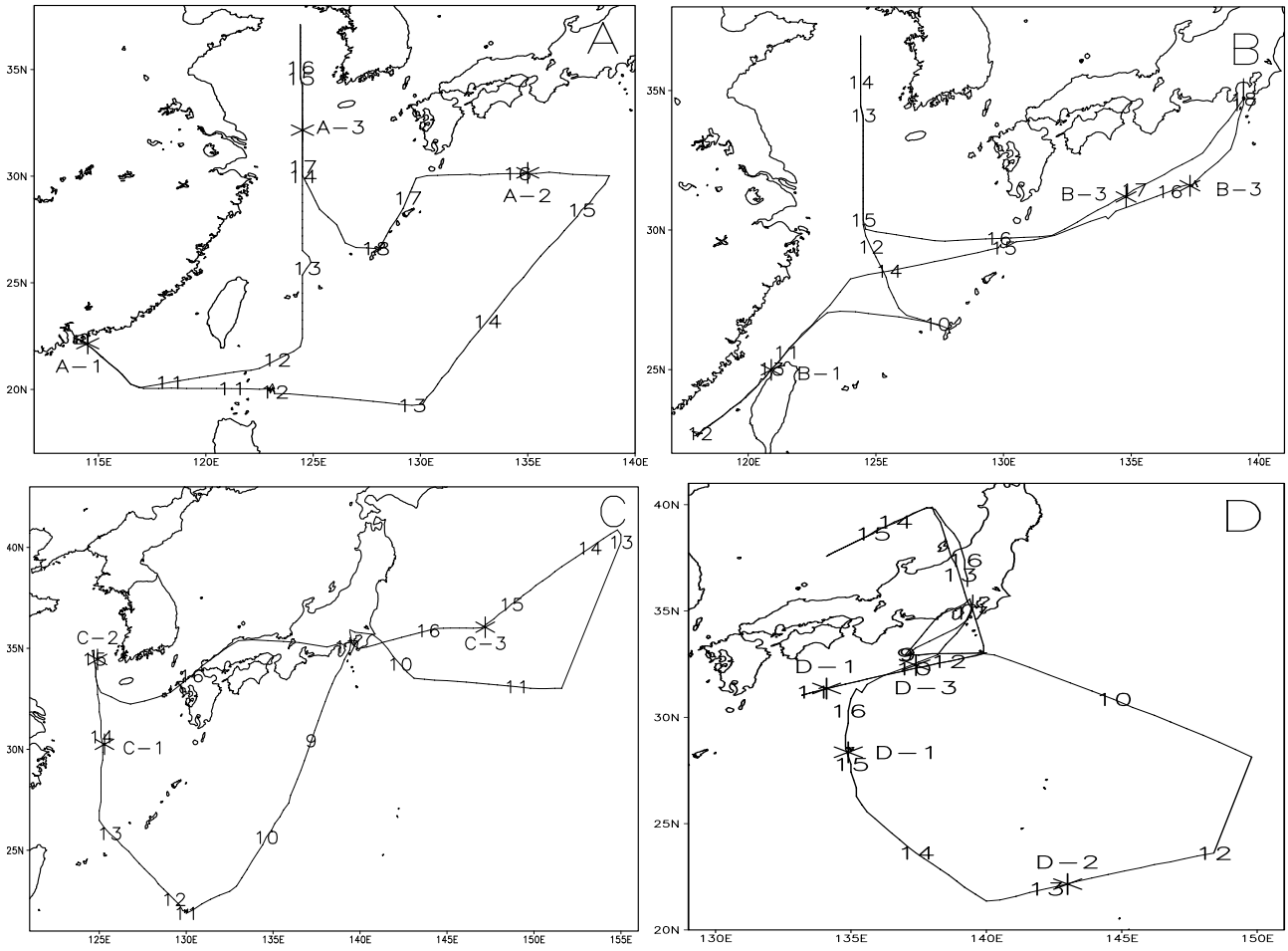
A
A−1
A−2
A−3
B
B−1
B−3
C
C−1
C−2
C−3
D
D−1
D−2
D−3

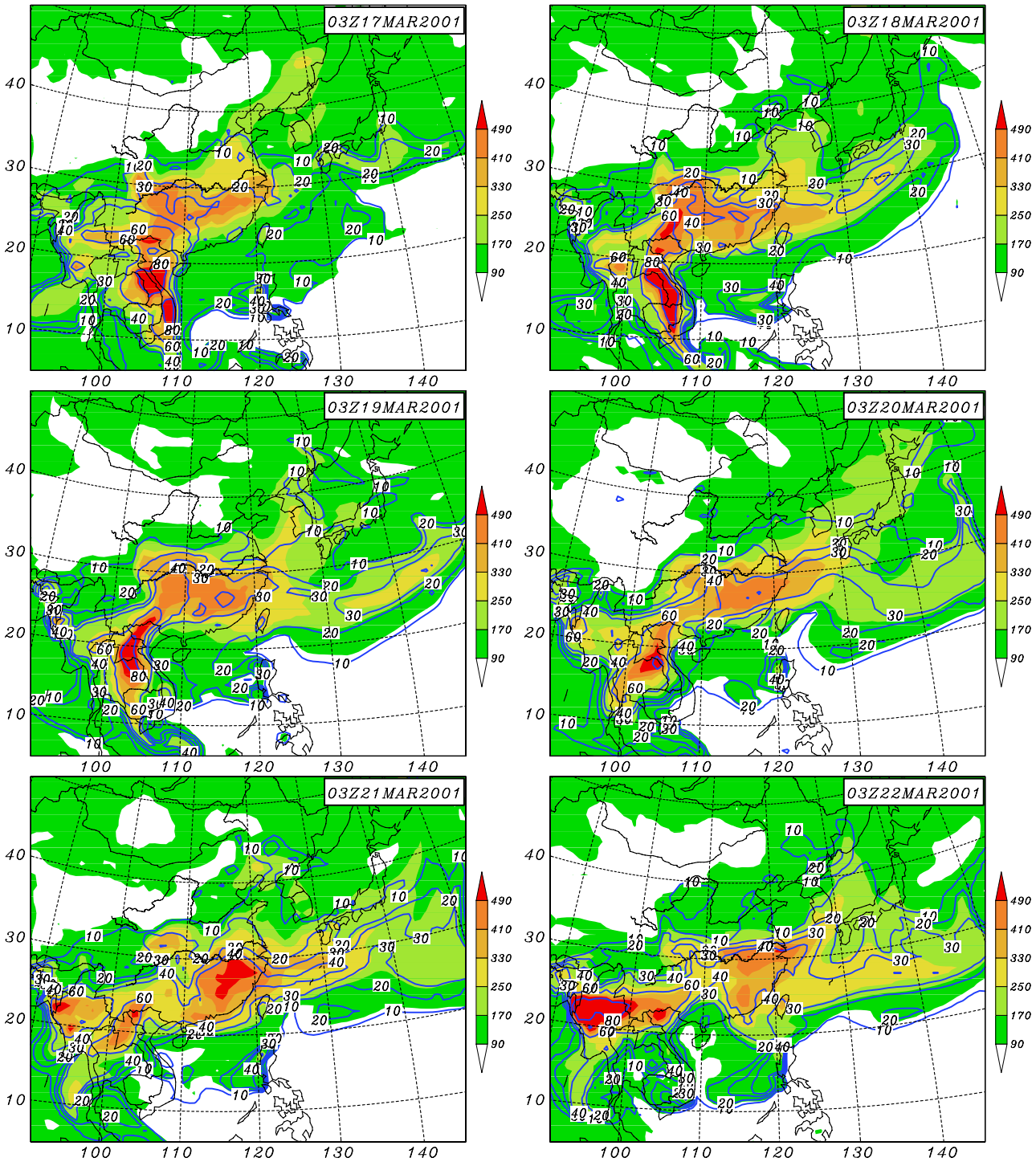

Figure 7. Horizontal distributions of average CO concentrations (shaded, ppbv) and the percentage contributions (contour with intervals 10, %) from biomass burning in the boundary layer (from surface to 1000 m) at 0300 Z (1200 JST) on March 17, 18, 20, 21, 23 and 24, 2001.

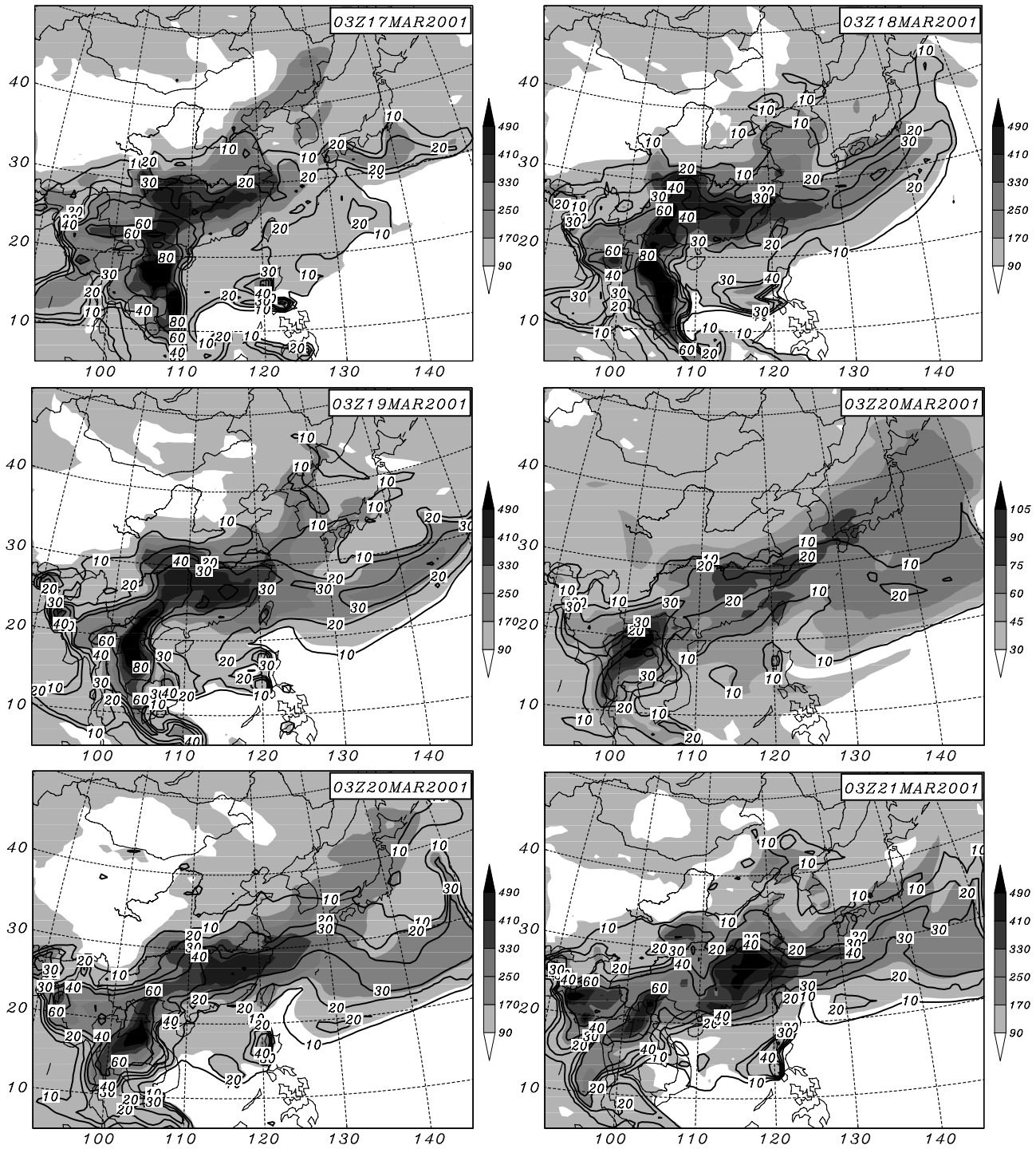
03Z17MAR2001
03Z18MAR2001
03Z19MAR2001
03Z20MAR2001
03Z20MAR2001
03Z21MAR2001
100
110
120
130
140
10
20
30
40
490
410
330
250
170
90
105
75
60
45

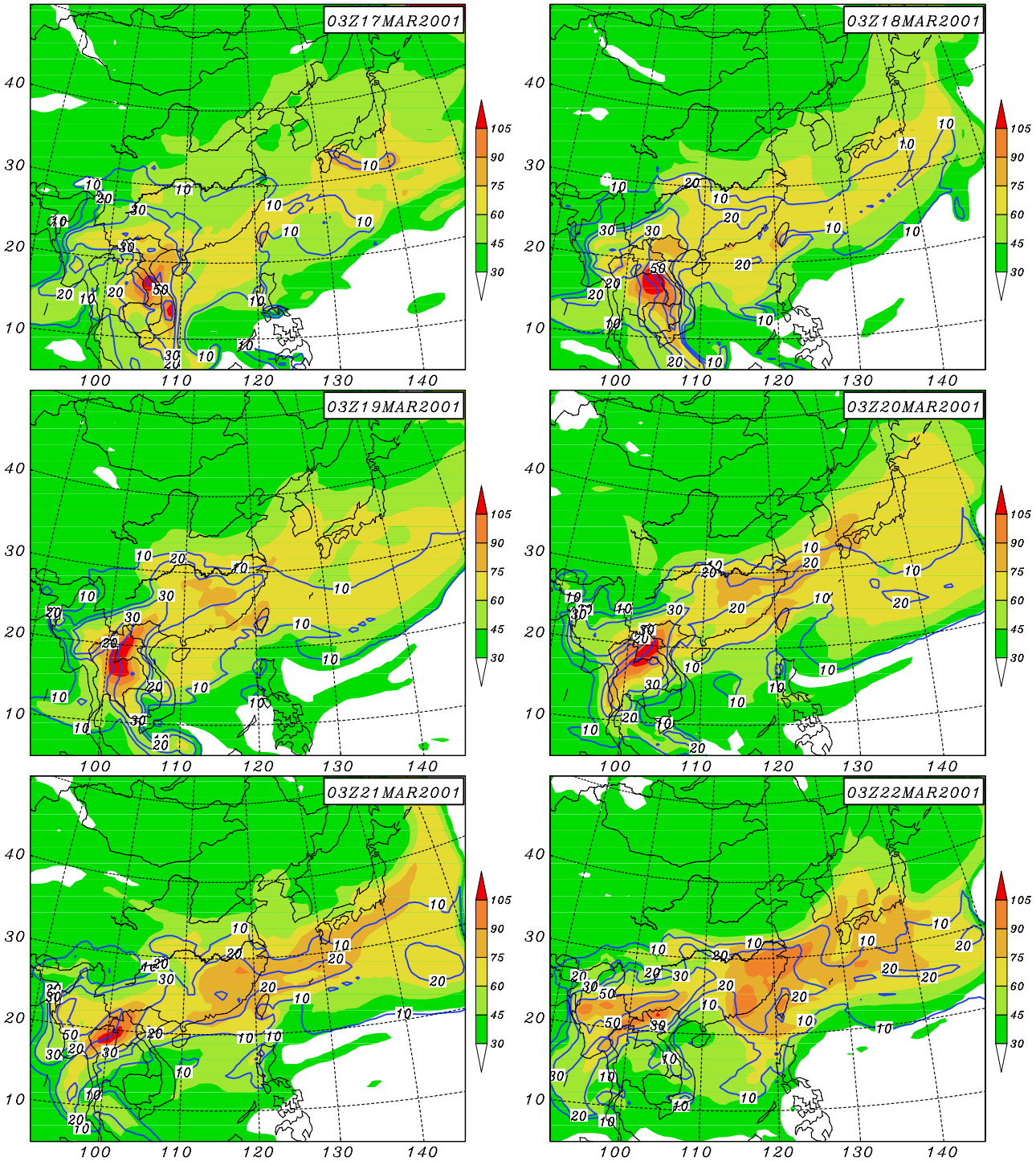

Figure 8. Horizontal distributions of average O_3 concentrations (shaded, ppbv) and the percentage contributions (contour with intervals 10, %) from biomass burning in the boundary layer (from surface to 1000 m) at 0300 Z (1200 JST) on March 17, 18, 20, 21, 23 and 24, 2001.

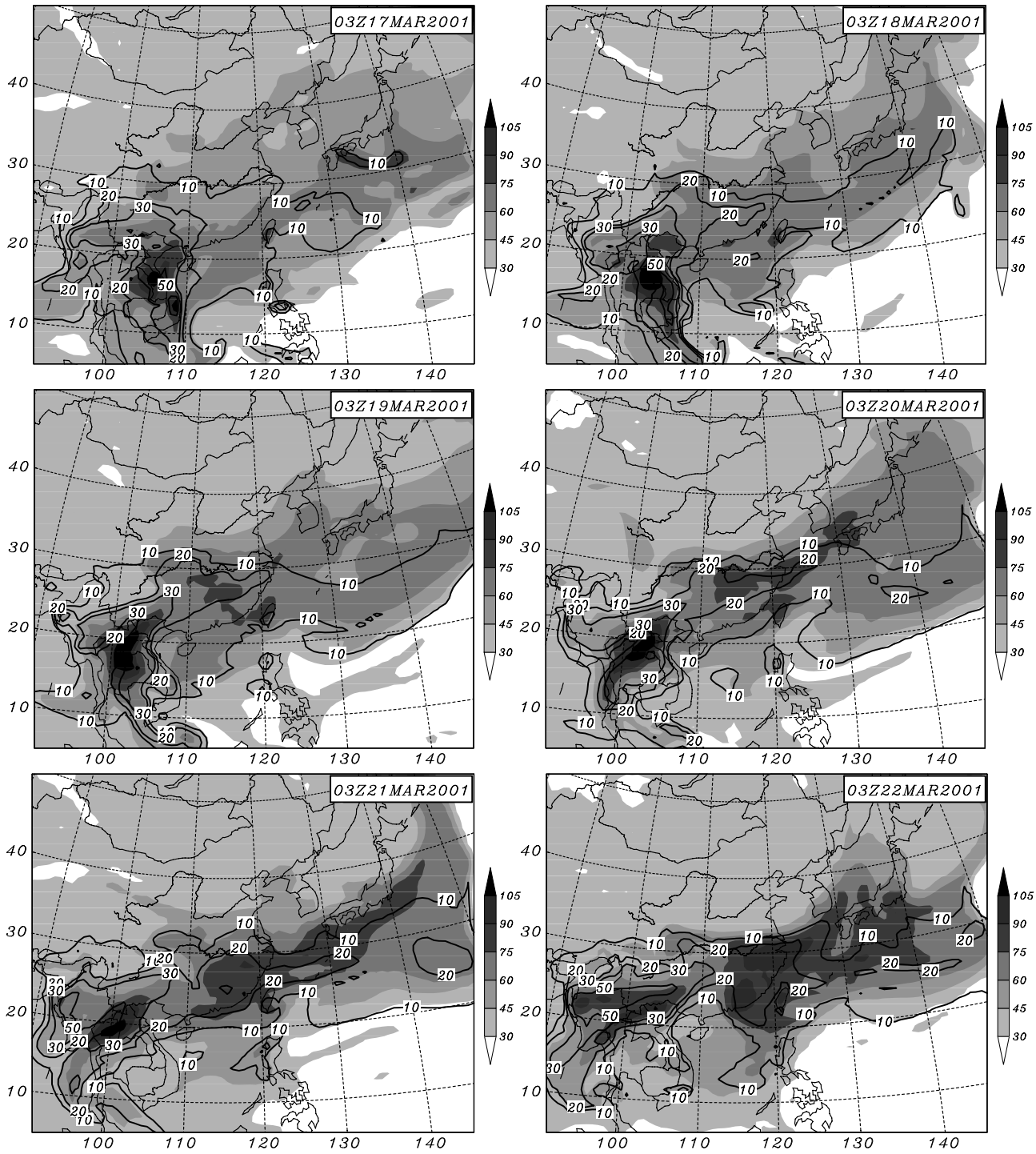
03Z17MAR2001
03Z18MAR2001
03Z19MAR2001
03Z20MAR2001
03Z21MAR2001
03Z22MAR2001
105
90
75
60
45
30
100
110
120
130
140
10
20
30
40

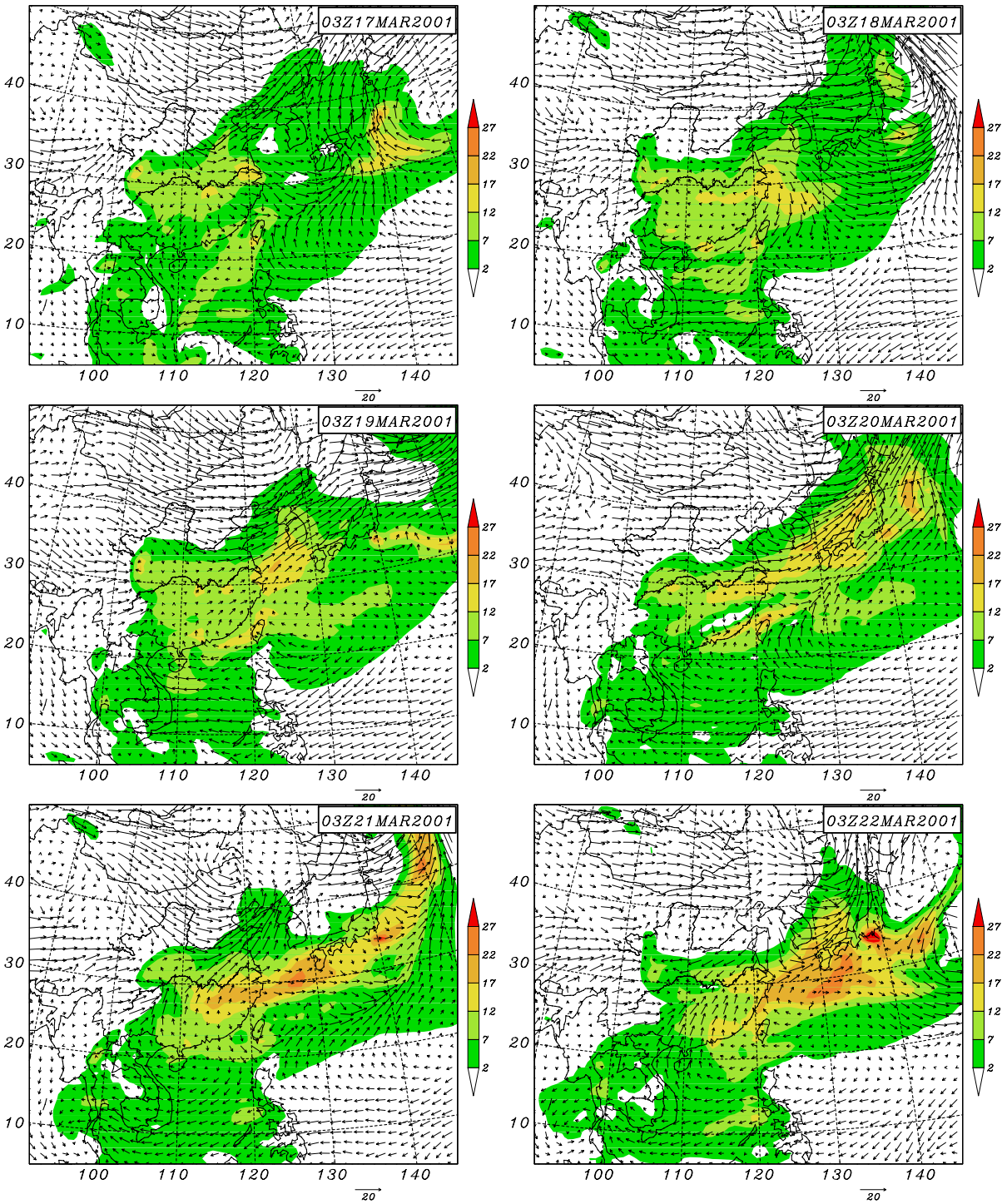

Figure 9. Horizontal distributions of average SO_4^{2-} concentrations (ug/m^3) in the boundary layer (from surface to 1000 m) at 0300 Z (1200 JST) on March 17, 18, 20, 21, 23 and 24, 2001. Also shown are wind vectors at an altitude of ~500 m.

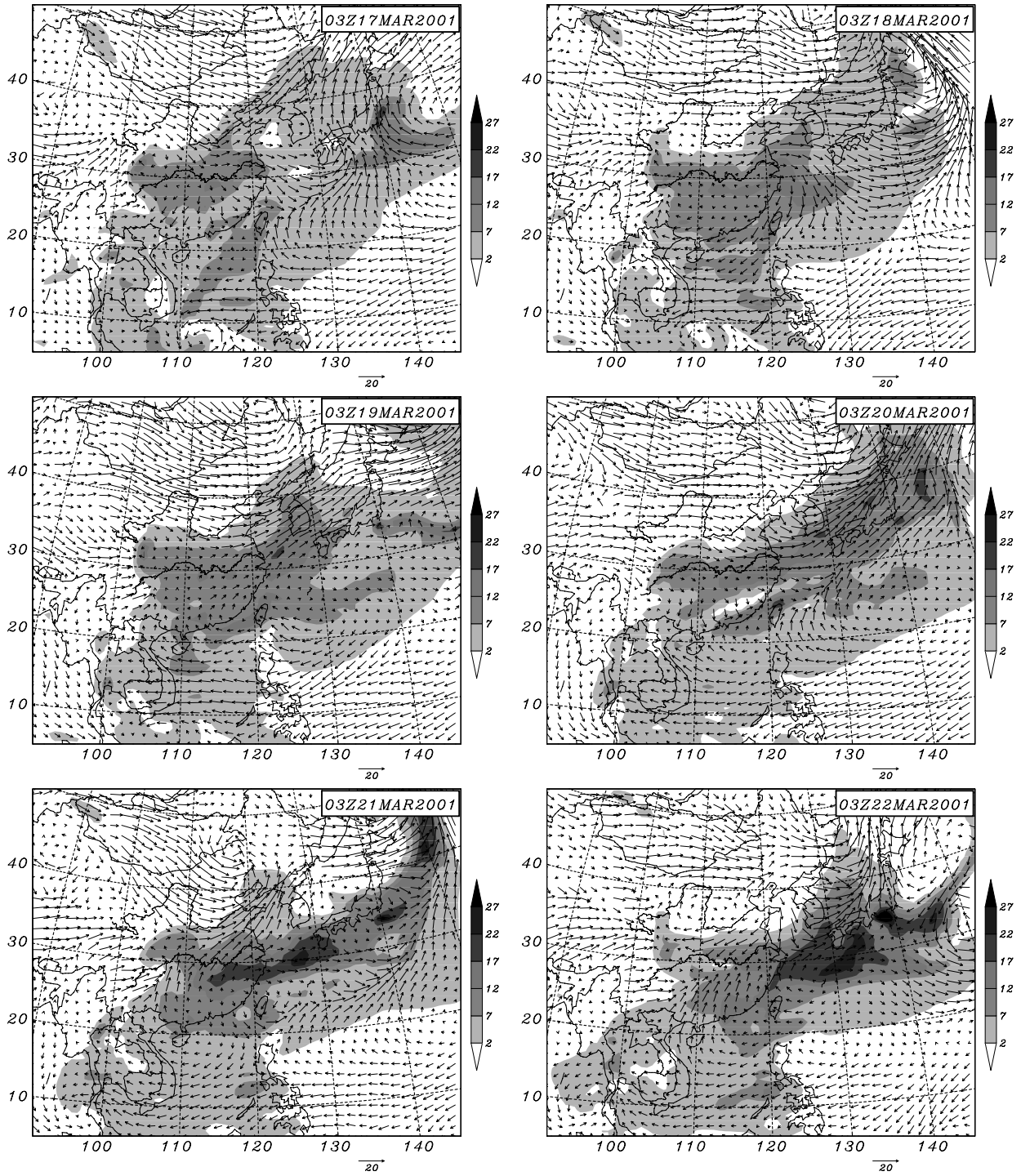
03Z17MAR2001
03Z18MAR2001
03Z19MAR2001
03Z20MAR2001
03Z21MAR2001
03Z22MAR2001
40
30
20
10
100
110
120
130
140
27
22
17
12
7
2
20

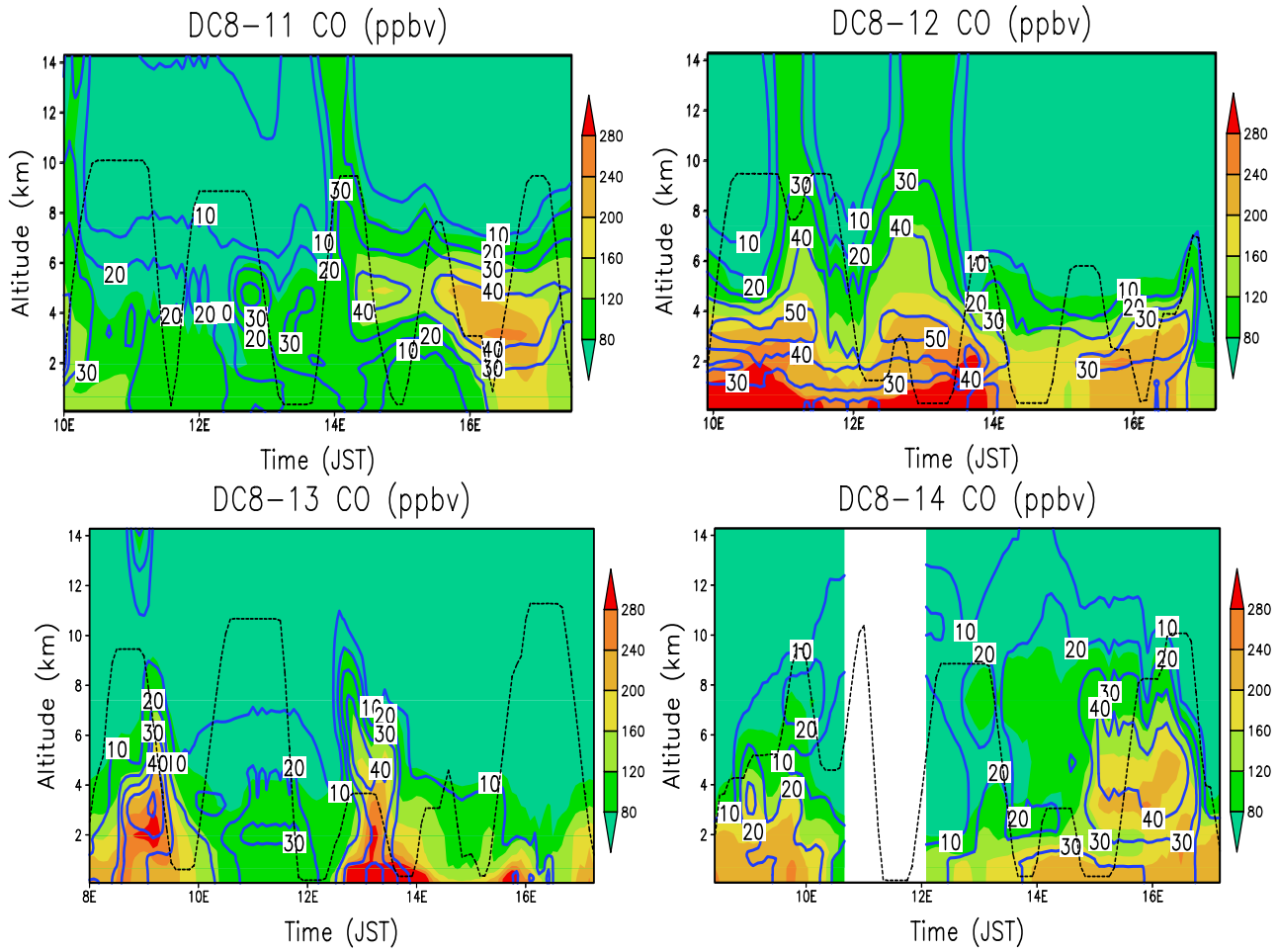

Figure 10. Vertical distributions of CO concentrations (ppbv, shaded) and the percentage contributions (%, contour) from biomass burning along the DC-8 flight tracks.

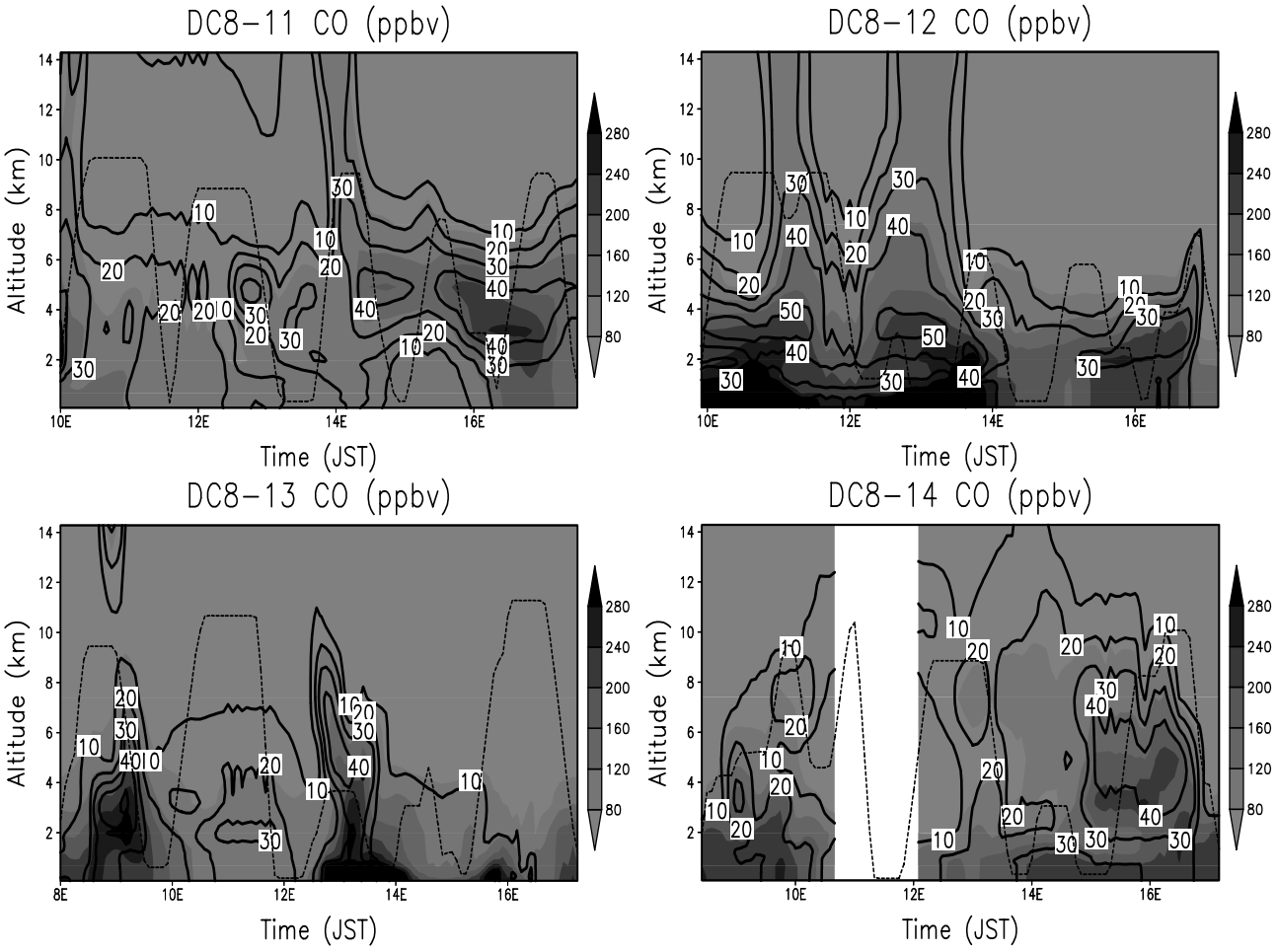
DC8-11 CO (ppbv)
DC8-12 CO (ppbv)
DC8-13 CO (ppbv)
DC8-14 CO (ppbv)
Altitude (km)
Time (JST)
10E
12E
14E
16E
8E
280
240
200
160
120
80

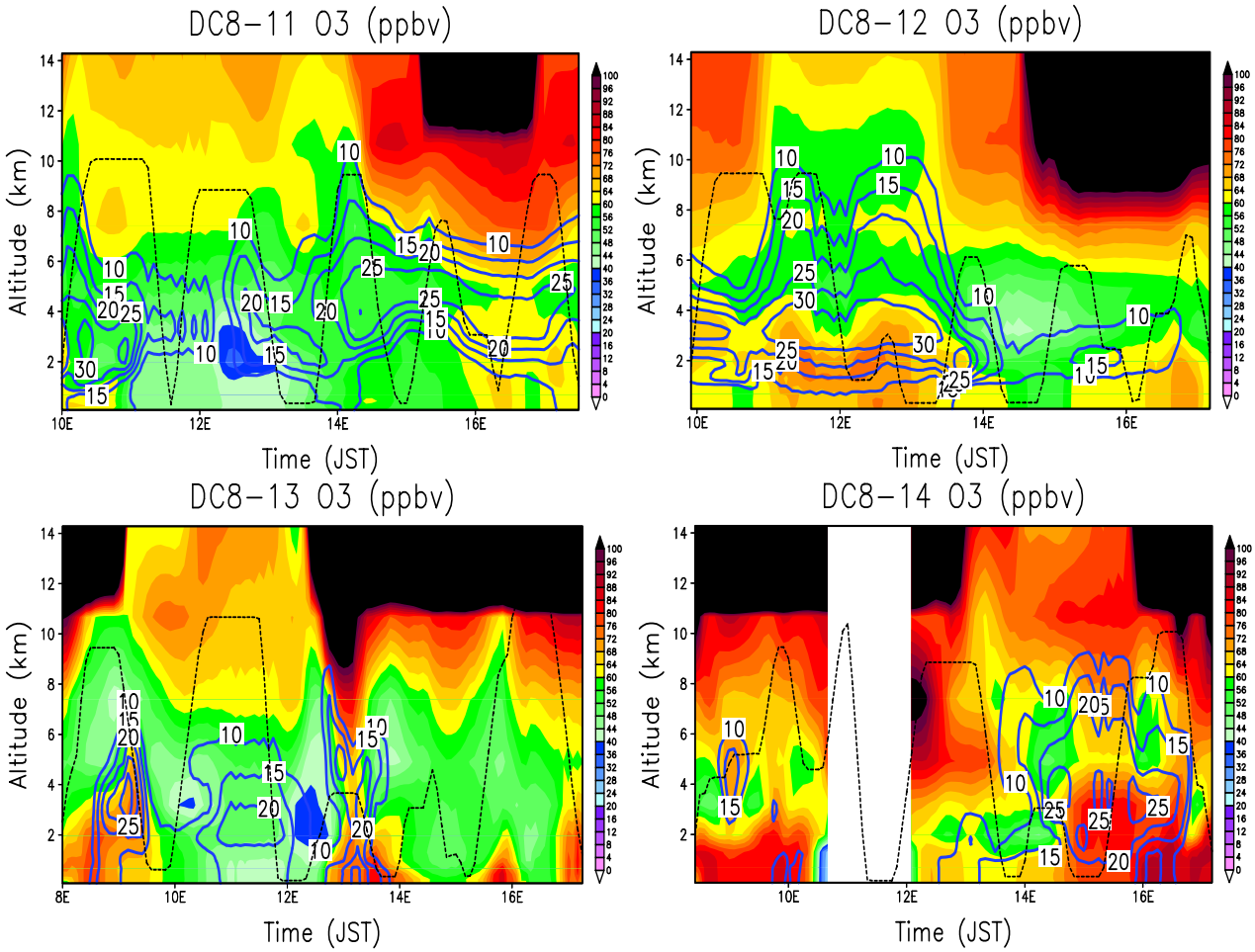

Figure 11. Vertical distributions of O_3 concentrations (ppbv, shaded) and the percentage contributions (%, contour) from biomass burning along the DC-8 flight tracks.

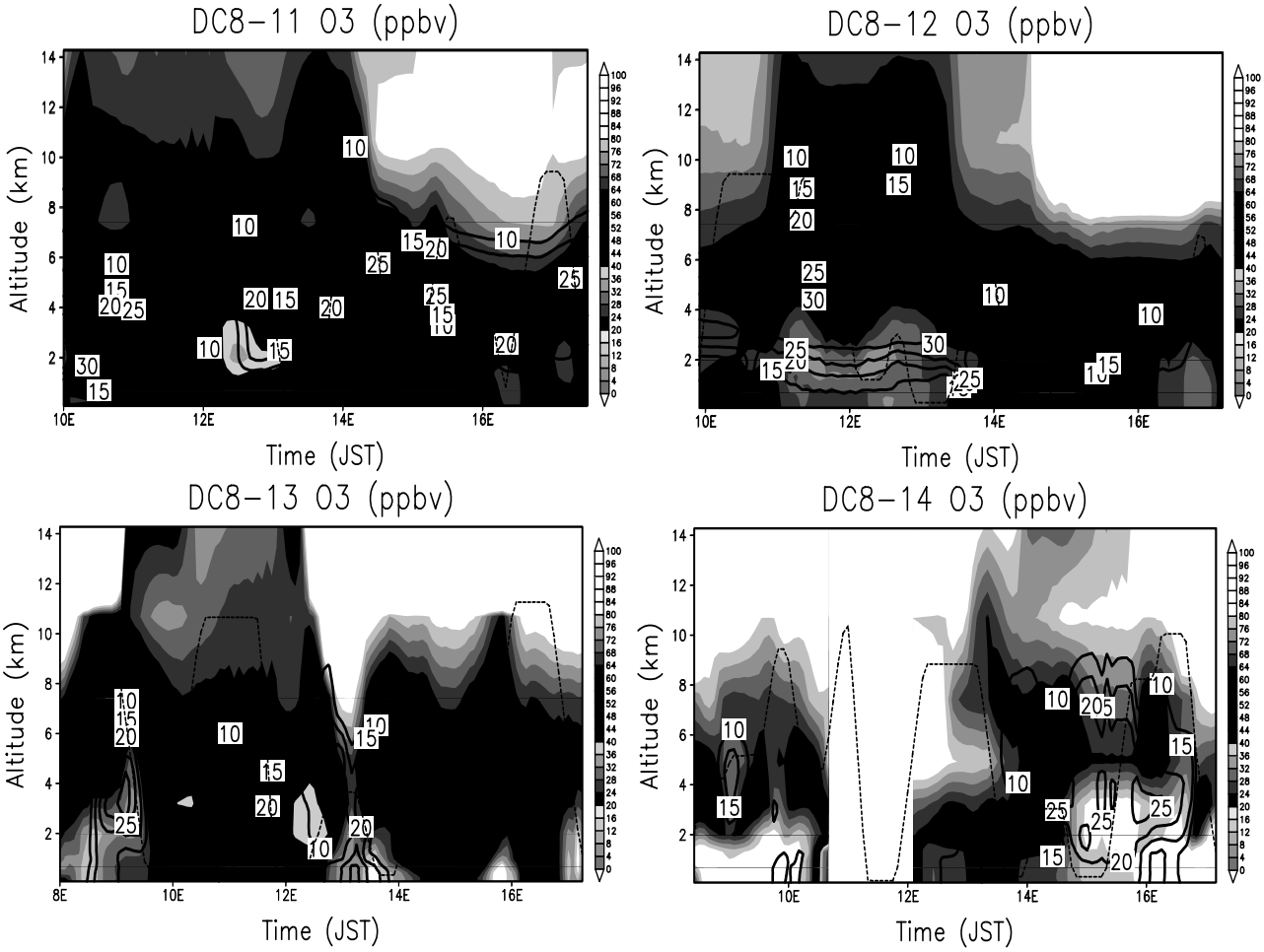
DC8-11 O3 (ppbv)
DC8-12 O3 (ppbv)
DC8-13 O3 (ppbv)
DC8-14 O3 (ppbv)
Altitude (km)
Time (JST)
10E
12E
14E
16E
8E

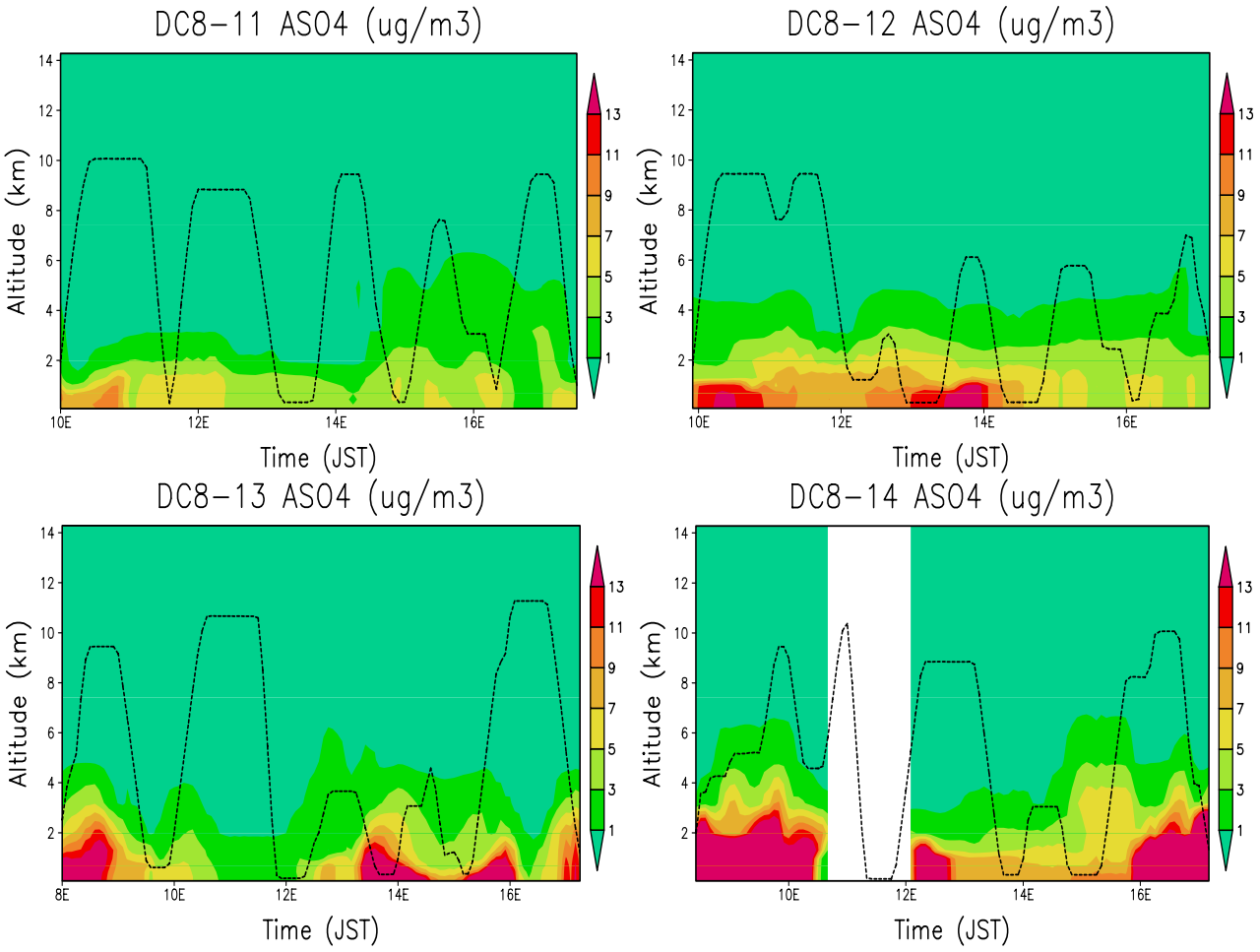

Figure 12. Vertical distributions of SO_4^{2-} concentrations (ug/m^3) along the DC-8 flight tracks.

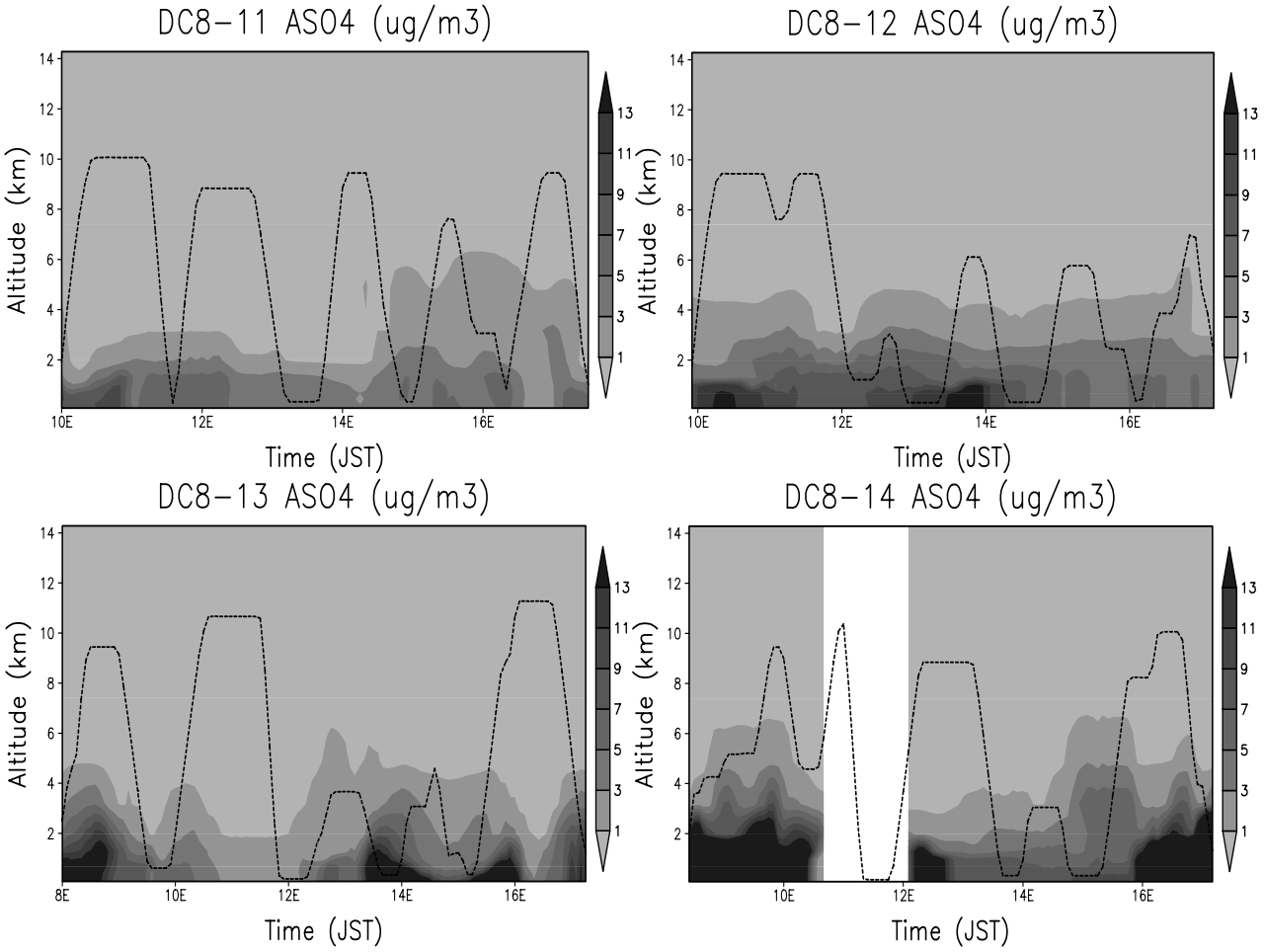
DC8-11 ASO4 (ug/m3)
DC8-12 ASO4 (ug/m3)
DC8-13 ASO4 (ug/m3)
DC8-14 ASO4 (ug/m3)
Altitude (km)
Time (JST)
8E
10E
12E
14E
16E
1
3
5
7
9
11
13

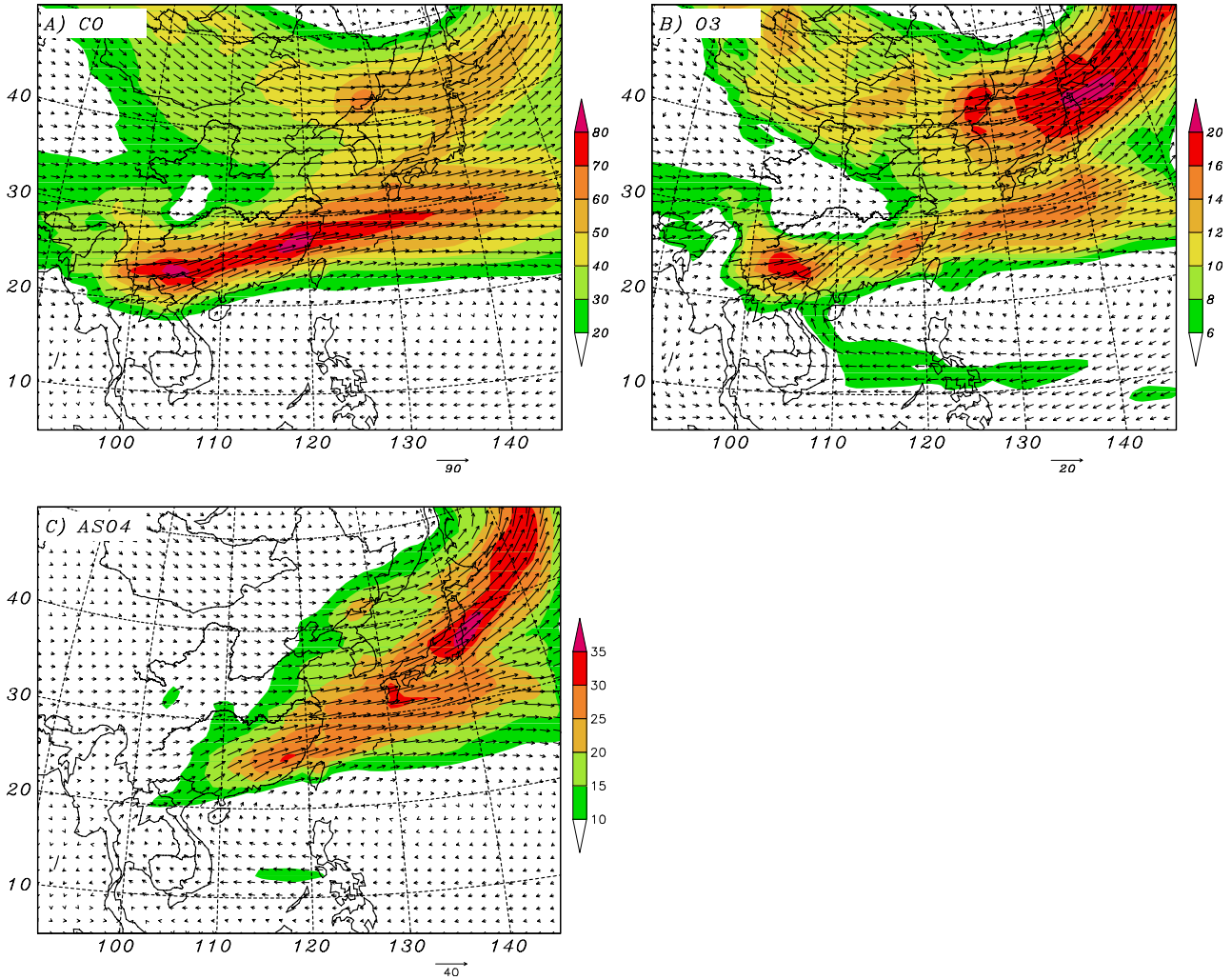

Figure 13. Average horizontal fluxes of (a) CO (10^{-5} mole/m^2/s), (b) O_3 (10^{-5} mole/m^2/s) and SO_4^{2-} (10^{-7} mole/m^2/s) and their magnitudes (shaded) vertically integrated from surface to 9 km except for O_3 to 2.5 km in the period March 17-24, 2001.

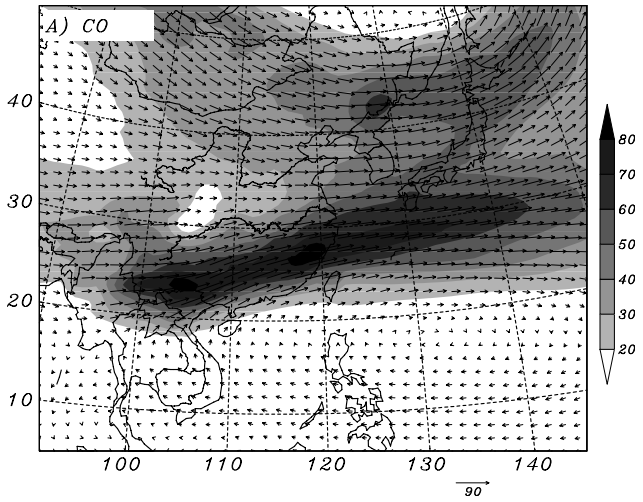
A) C0
40
30
20
10
100
110
120
130
140
90
80
70
60
50
40
30
20

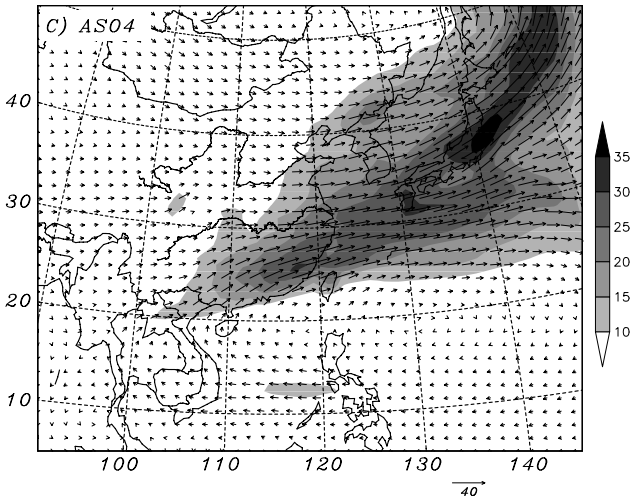
C) AS04
40
30
20
10
100
110
120
130
140
40
35
30
25
20
15
10

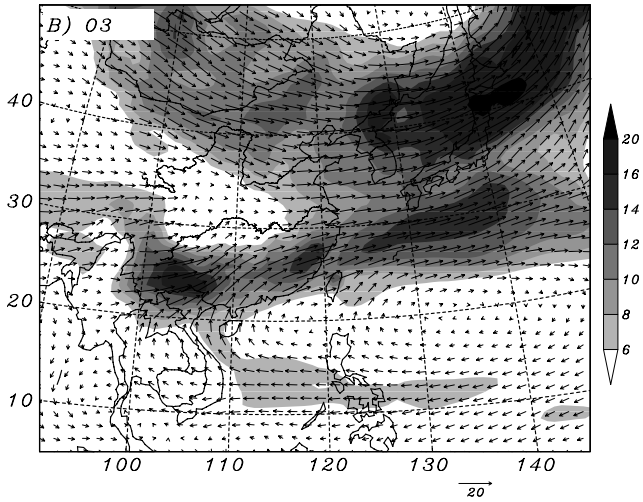
B) 03
40
30
20
10
100
110
120
130
140
20
20
16
14
12
10
8
6

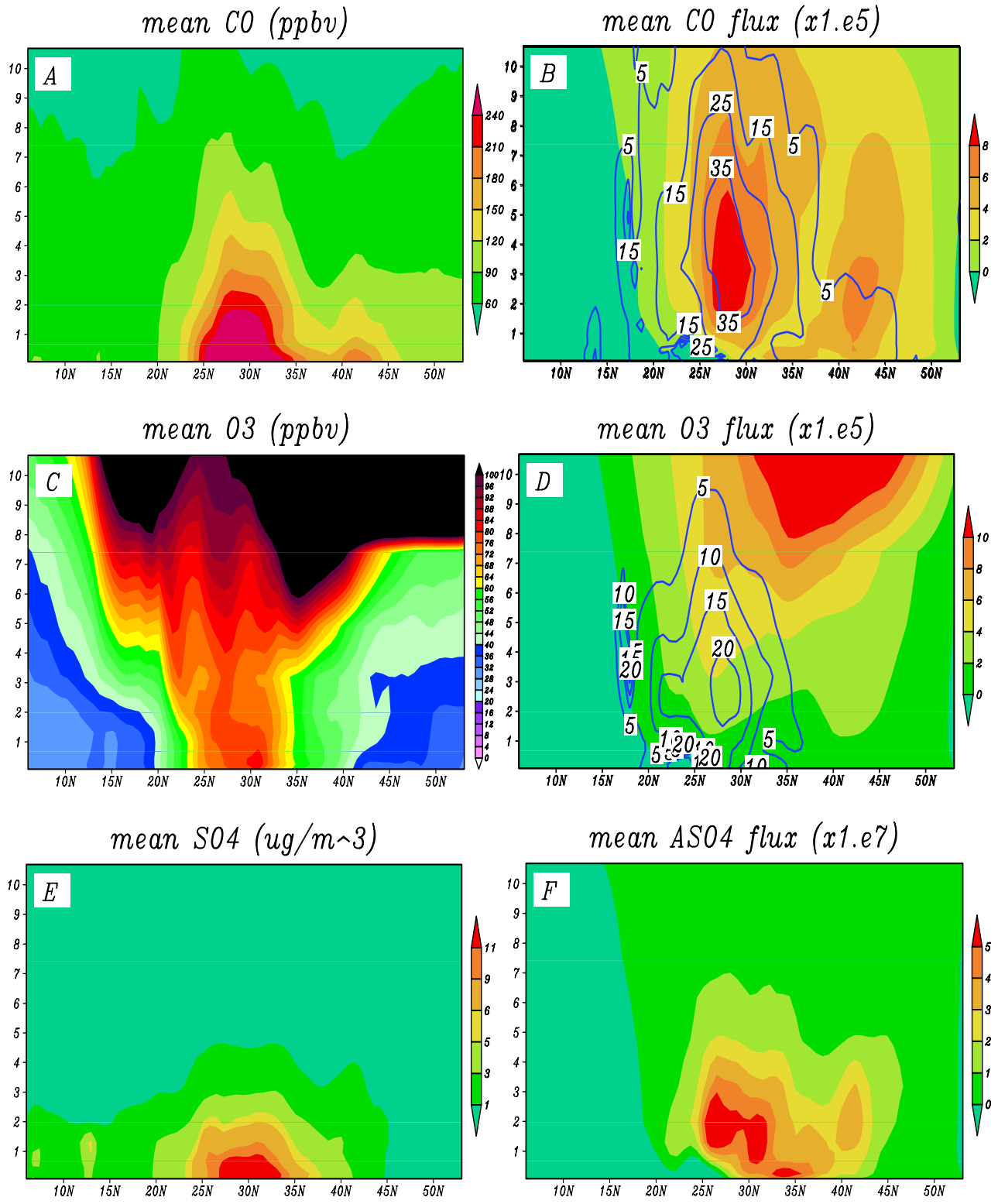

Figure 14. Average concentrations of (a) CO (ppbv), (c) O3 (ppbv) and (e) SO_4^{2-} (ug/m^3) and zonal fluxes of (b) CO (shaded, 10^{-5}mole/m^2/s) and (d) O_3 (shaded, 10^{-5}mole/m^2/s) with their percentage contributions from biomass burning (contour, %) and (f) SO_4^{2-} (shaded, 10^{-7}mole/m^2/s) in the period

March 17-24, 2001, along ~125°E.